

# Axisymmetric black hole in a non–commutative gauge theory: classical and quantum gravity effects

A. A. Araújo Filho,<sup>1,\*</sup> N. Heidari,<sup>2,†</sup> and Ali Övgün<sup>3,‡</sup>

<sup>1</sup>*Departamento de Física, Universidade Federal da Paraíba,  
Caixa Postal 5008, 58051–970, João Pessoa, Paraíba, Brazil.*

<sup>2</sup>*Center for Theoretical Physics, Khazar University,  
41 Mehseti Street, Baku, AZ-1096, Azerbaijan.*

<sup>3</sup>*Physics Department, Eastern Mediterranean University,  
Famagusta, 99628 North Cyprus via Mersin 10, Türkiye.*

(Dated: February 18, 2025)

This work explores both classical and quantum aspects of an axisymmetric black hole within a non–commutative gauge theory. The rotating solution is derived using a modified Newman–Janis procedure. The analysis begins with the horizon structure, ergospheres, and angular velocity. The thermodynamic properties are examined through surface gravity, focusing on the Hawking temperature, entropy, and heat capacity. In addition, the remnant mass is calculated. The Hawking radiation is treated as a tunneling process for bosonic and fermionic particles, along with the corresponding particle creation density. Geodesic motion is explored, emphasizing null geodesics, radial accelerations, the photon sphere, and black hole shadows. Finally, the gravitational lensing in the strong deflection limit is investigated.

---

\* [dilto@fisica.ufc.br](mailto:dilto@fisica.ufc.br)

† [heidari.n@gmail.com](mailto:heidari.n@gmail.com)

‡ [ali.ovgun@emu.edu.tr](mailto:ali.ovgun@emu.edu.tr)

**CONTENTS**

I. Introduction	3
II. Black hole in a non–comutative gauge theory	5
III. A corrected Newman–Janis technique	9
IV. The general remarks and thermal behavior	12
A. The horizons and the corresponding ergosheres	12
B. The angular velocity	13
C. The surface gravity	15
D. The Hawking temperature	17
E. The remnant mass	18
F. The entropy	19
G. Heat capacity	19
V. Hawking radiation as a tunneling process	20
A. Bosonic particle modes	20
B. Fermionic particle modes	24
VI. Geodesics	27
A. The radial acceleration analysis for null geodesics	30
VII. Shadows	32
VIII. Gravitational lensing in the strong deflection regime	35
IX. Conclusion	42
Acknowledgments	43
References	43

## I. INTRODUCTION

Within general relativity, the geometry of spacetime does not impose a definitive lower limit on measurable distances. The Planck length, however, is commonly regarded as a fundamental constraint. To explore the implications of this limitation, non-commutative spacetimes have been proposed as a theoretical framework. This concept, which is connected to string theory and other quantum gravity models, has become increasingly relevant in the study of supersymmetric field theories, especially through the lens of superfield formalism [1–6]. In addition, a prominent technique for incorporating non-commutative structures into gravitational models is the Seiberg–Witten map, which facilitates the gauging of specific symmetry groups [7]. Such a formalism has been used to study black hole thermodynamics, evaporation, and thermal behavior, including emission spectra and thermal state quantities [8–15].

The exploration of non-commutative effects in gravitational systems has seen significant progress with the alteration of matter sources in Einstein’s field equations, maintaining the form of the Einstein tensor unchanged [16]. This approach substitutes the conventional point-mass density with smoothly distributed profiles, such as Gaussian [17] and Lorentzian functions [18]. Such modifications have fueled extensive research into black hole thermodynamics, including analyses of thermal radiation and quantum tunneling processes [8, 9, 19]. They have also been applied to topological studies within Gauss–Bonnet gravity [20], black hole shadow formation [21–23], and phenomena like matter accretion and gravitational lensing [24–26]. Recent efforts have explored non-commutativity as a perturbative correction in gravitational frameworks, expanding its theoretical implications [27].

Gravitational waves are essential for understanding a range of physical phenomena, from early universe dynamics to stellar processes such as oscillations and binary interactions [28–34]. The intensity and mode of these waves fluctuate, while their spectral features convey details about their sources [35]. Black holes stand out as prominent emitters, generating radiation during their formation, with distinct frequencies known as *quasinormal* modes [36–54]. The analysis of these modes in black hole physics often employs the weak field approximation, a method utilized not only within the scope of general relativity but also in various alternative gravitational frameworks, including those exploring Lorentz symmetry violations and extended theoretical models [55–84].

The imaging of the supermassive black hole at the core of the M87 galaxy by the Event Horizon Telescope has drawn considerable scientific focus [81, 85–94]. Virbhadra and Ellis were among the first to propose a simplified lensing formula for supermassive black holes in asymptotically flat spacetimes, revealing how strong gravitational fields create multiple images symmetrically distributed along the optical axis [95, 96]. Analytical techniques for examining strong gravitational lensing were later expanded by Frittelli et al. [97], Bozza et al. [98], and Tsukamoto [99], leading to more comprehensive studies of light deflection. Investigations have since extended to various frameworks, such as Reissner–Nordström backgrounds [100–104], axisymmetric black holes [105–110], exotic objects like wormholes [111–115], and spacetime modifications arising from alternative gravity theories [116–119].

Hawking introduced a fundamental concept linking quantum mechanics with gravity, contributing to the foundation of quantum gravity research [120–122]. He demonstrated that black holes can emit thermal radiation, causing a gradual loss of mass, a phenomenon now known as Hawking radiation [123–128]. This result, derived from quantum field theory in curved spacetime near the event horizon, has significantly influenced the study of black hole thermodynamics and quantum effects [49, 129–137]. Kraus and Wilczek [138], later expanded by Parikh and Wilczek [120, 139, 140], reinterpreted *Hawking* radiation as a quantum tunneling effect within a semi-classical framework. This perspective has since been extensively explored in the context of various black hole configurations [141–152].

The Newman–Janis method, designed to incorporate angular momentum into static spacetimes, offers a widely applied approach for generating rotating black hole solutions from spherically symmetric metrics [153, 154]. This technique relies on a complex coordinate transformation and has been instrumental in deriving the Kerr-like solutions from simpler static models, such as the Schwarzschild-like spacetimes. Recognizing the limitations of the original formulation, recent works have been used modified versions to extend its applicability to a broader spectrum of gravitational scenarios [155].

An alternative to the standard Newman–Janis procedure, known as the modified Newman–Janis algorithm [156, 157], avoids the conventional complexification process, which has long been a topic of debate. This revised method instead employs a more geometrically motivated transformation, providing a clearer interpretation of the process. It has been particularly effective in deriving rotating metrics for spacetimes with imperfect fluids, broadening the scope of the original approach, which primarily addressed perfect fluid models. By ap-

plying this modified technique, rotating solutions can be obtained from static, spherically symmetric metrics in a wider range of physical contexts, enhancing its versatility across gravitational models [155, 158–163].

This work examines an axisymmetric black hole within a non-commutative gauge theory, emphasizing both its classical structure and quantum properties. The rotating solution is obtained through a modified Newman–Janis procedure, with the horizon structure, ergospheres, and angular velocity studied as fundamental aspects of the spacetime geometry. The thermodynamic behavior is characterized by surface gravity, from which the Hawking temperature, entropy, and heat capacity are determined. Furthermore, the remnant mass is also addressed. Quantum effects are addressed by modeling Hawking radiation as a tunneling process for bosonic and fermionic particles. The motion of test particles is explored through a detailed geodesic analysis, including null trajectories, radial accelerations, the photon sphere, and the formation of black hole shadows. Finally, the gravitational lensing is examined in the strong deflection regime.

## II. BLACK HOLE IN A NON-COMMUTATIVE GAUGE THEORY

This section outlines the essential framework for examining the non-commutative gauge theory of gravity. As previously noted, the gauge group involved is the de Sitter group,  $SO(4, 1)$ . To set the stage, we will first describe the formulation of the  $SO(4, 1)$  gauge theory in a commutative  $(3 + 1)$ -dimensional Minkowski spacetime, where the metric in spherical coordinates takes the form

$$ds^2 = dr^2 + r^2 d\Omega_2^2 - c^2 dt^2, \quad (1)$$

where  $d\Omega_2^2 = d\theta^2 + \sin^2\theta d\varphi^2$ . The group  $SO(4, 1)$  consists of ten generators, denoted by  $\mathcal{M}_{\mathcal{AB}}$ , which satisfy the antisymmetry relation  $\mathcal{M}_{\mathcal{AB}} = -\mathcal{M}_{\mathcal{BA}}$ . The indices involved are  $\mathcal{A}, \mathcal{B} = a, 5$  with  $a, b = 0, 1, 2, 3$ . These generators decompose into two distinct sets: the components  $\mathcal{M}_{ab} = -\mathcal{M}_{ba}$ , responsible for rotations, and the components  $\mathcal{P}_a = \mathcal{M}_{a5}$ , which describe translations.

The undeformed gauge potentials are denoted by  $\omega_\mu^{AB}(x)$ , which satisfy the antisymmetric condition  $\omega_\mu^{AB}(x) = -\omega_\mu^{BA}(x)$ . These potentials are distinct from the spin connection, expressed as  $\omega_\mu^{ab}(x) = -\omega_\mu^{ba}(x)$ , and the tetrad fields, denoted by  $e_\mu^a(x)$ . The components

$\hat{\omega}_\mu^{a5}(x)$  are related to the tetrad fields through the expression  $\hat{\omega}_\mu^{a5}(x) = \mathcal{K}\hat{e}_\mu^a(x)$ , where  $\mathcal{K}$  represents a contraction parameter. Additionally, another gauge field can be defined as  $\hat{\omega}_\mu^{55}(x) = \mathcal{K}\hat{\phi}_\mu(x, \Theta)$ , where the field  $\hat{\phi}_\mu(x, \Theta)$  vanishes when the limit  $\mathcal{K} \rightarrow 0$  is taken. This limiting case effectively reduces the gauge group to the Poincaré group  $\text{ISO}(3, 1)$  [164, 165]. The corresponding field strength associated with the gauge potential  $\omega_\mu^{AB}(x)$  is given by

$$F_\mu^{AB} = \partial_\mu \omega_\nu^{AB} - \partial_\nu \omega_\mu^{AB} + (\omega_\mu^{AC} \omega_\nu^{DB} - \omega_\nu^{AC} \omega_\mu^{DB}) \eta_{CD} \quad (2)$$

where  $\mu, \nu = 0, 1, 2, 3$  and the metric tensor is defined as  $\eta_{AB} = \text{diag}(+, +, +, -, +)$ . Furthermore, the expression can be rewritten as

$$F_{\mu\nu}^{a5} = \mathcal{K} [\partial_\mu e_\nu^a - \partial_\nu e_\mu^a + (\omega_\mu^{ab} e_\nu^a - \omega_\nu^{ab} e_\mu^a) \eta_{bc}] = \mathcal{K} T_{\mu\nu}^a, \quad (3a)$$

$$F_{\mu\nu}^{ab} = \partial_\mu \omega_\nu^{ab} - \partial_\nu \omega_\mu^{ab} + (\omega_\mu^{ac} \omega_\nu^{db} - \omega_\nu^{ac} \omega_\mu^{db}) \eta_{cd} + \mathcal{K} (e_\mu^a e_\nu^b - e_\nu^a e_\mu^b) = R_{\mu\nu}^{ab}, \quad (3b)$$

where  $\eta_{ab} = \text{diag}(+, +, +, -)$ . It is important to highlight that the Poincaré gauge group being considered here is linked to the geometric structure of Riemann–Cartan spacetime, which incorporates both curvature and torsion fields [164, 166]. The torsion tensor, defined as  $T_{\mu\nu}^a \equiv F_{\mu\nu}^{a5}/\mathcal{K}$ , and the curvature tensor, expressed as  $R_{\mu\nu}^{ab} \equiv F_{\mu\nu}^{ab}$ , are described in terms of the tetrad fields  $e_\mu^a(x)$  and the spin connection  $\omega_\mu^{ab}(x)$ . When the torsion field vanishes, as indicated by Eq. (3a), the spin connection can be determined solely from the tetrad fields.

Next, we consider a possible configuration for spherically symmetric gauge fields associated with the  $\text{SO}(4, 1)$  group [164, 166]:

$$e_\mu^1 = \left( \frac{1}{\mathcal{A}}, 0, 0, 0 \right), \quad e_\mu^2 = (0, r, 0, 0), \quad e_\mu^3 = (0, 0, r \sin\theta, 0), \quad e_\mu^0 = (0, 0, 0, \mathcal{A}), \quad (4)$$

and

$$\begin{aligned} \omega_\mu^{12} &= (0, \mathcal{W}, 0, 0), & \omega_\mu^{13} &= (0, 0, \mathcal{Z} \sin\theta, 0), & \omega_\mu^{10} &= (0, 0, 0, \mathcal{U}), \\ \omega_\mu^{23} &= (0, 0, -\cos\theta, \mathcal{V}), & \omega_\mu^{20} &= \omega_\mu^{30} = (0, 0, 0, 0), \end{aligned} \quad (5)$$

with  $\mathcal{A}$ ,  $\mathcal{U}$ ,  $\mathcal{V}$ ,  $\mathcal{W}$ , and  $\mathcal{Z}$  are functions dependent solely on the three-dimensional radial coordinate. Moreover, the non-vanishing components of the torsion tensor can be expressed as [165]

$$\begin{aligned} T_{01}^0 &= -\frac{\mathcal{A}\mathcal{A}' + \mathcal{U}}{\mathcal{A}}, & T_{03}^2 &= r \mathcal{V} \sin\theta T_{12}^2 = \frac{\mathcal{A} + \mathcal{W}}{\mathcal{A}}, \\ T_{02}^3 &= -r \mathcal{V}, & T_{13}^3 &= \frac{(\mathcal{A} + \mathcal{Z}) \sin\theta}{\mathcal{A}}, \end{aligned} \quad (6)$$

and, therefore, the curvature tensor reads [165]

$$\begin{aligned} R_{01}^{01} &= \mathcal{U}', & R_{01}^{23} &= -\mathcal{V}', & R_{23}^{13} &= (\mathcal{Z} - \mathcal{W}) \cos\theta, & R_{01}^{01} &= -\mathcal{U}\mathcal{W}, & R_{01}^{13} &= -\mathcal{V}\mathcal{W}, \\ R_{03}^{03} &= -\mathcal{U}\mathcal{Z}\sin\theta, & R_{03}^{12} &= \mathcal{V}\mathcal{Z}\sin\theta & R_{12}^{12} &= \mathcal{W}', & R_{23}^{23} &= (1 - \mathcal{Z}\mathcal{W}) \sin\theta, & R_{13}^{13} &= \mathcal{Z}'\sin\theta. \end{aligned} \quad (7)$$

The symbols  $\mathcal{A}'$ ,  $\mathcal{U}'$ ,  $\mathcal{V}'$ ,  $\mathcal{W}'$ , and  $\mathcal{Z}'$  indicate derivatives taken with respect to the radial coordinate. To ensure the torsion field is absent, as outlined in Eq. (6), the following conditions are proposed:

$$\mathcal{V} = 0, \quad \mathcal{U} = -\mathcal{A}\mathcal{A}', \quad \mathcal{W} = -\mathcal{A} = \mathcal{Z}. \quad (8)$$

Taking into account the field equation

$$R_{\mu}^a - \frac{1}{2}R e_{\mu}^a = 0, \quad (9)$$

expressed through the tetrad fields  $e_{\mu}^a(x)$ , with the definitions  $R_{\mu}^a = R_{\mu\nu}^{ab}e_b^{\nu}$  and  $R = R_{\mu\nu}^{ab}e_a^{\mu}e_b^{\nu}$ , the resulting solution can be written as

$$\mathcal{A}(r) = \sqrt{1 - \frac{\alpha}{r}}, \quad (10)$$

where the constant  $\alpha$  is defined as  $\alpha = 2GM/c^2$ , with  $G$  denoting the gravitational constant,  $M$  the black hole mass, and  $c$  the speed of light. To obtain the modified metric  $ds^2 = \hat{g}_{\mu\nu}(x, \Theta)dx^{\mu}dx^{\nu}$ , expressed in spherical coordinates  $x^{\mu} = (r, \theta, \varphi, ct)$  for a (3+1)–dimensional non–commutative Schwarzschild spacetime, it is necessary to determine the deformed tetrad fields  $\hat{e}_{\mu}^a(x, \Theta)$ . These tetrads emerge from a contraction between the non–commutative gauge group  $SO(4, 1)$  and the Poincaré group  $ISO(3, 1)$ , employing the Seiberg–Witten map formalism [4, 167, 168]. The structure of the non–commutative spacetime can then be defined under the following conditions:

$$[x^{\mu}, x^{\nu}] = i\Theta^{\mu\nu}. \quad (11)$$

The constants  $\Theta^{\mu\nu}$  are assumed to be real and satisfy the antisymmetric relation  $\Theta^{\mu\nu} = -\Theta^{\nu\mu}$ . As a result, the gravitational fields, specifically the modified tetrad fields  $\hat{e}_{\mu}^a(x, \Theta)$  and the gauge connection  $\hat{\omega}_{\mu}^{AB}(x, \Theta)$ , within a non–commutative spacetime, can be expanded as a power series in the parameter  $\Theta$  [4, 164, 165, 167].

$$\begin{aligned} \hat{e}_{\mu}^a(x, \Theta) &= e_{\mu}^a(x) - i\Theta^{\nu\rho}e_{\mu\nu\rho}^a(x) + \Theta^{\nu\rho}\Theta^{\lambda\tau}e_{\mu\nu\rho\lambda\tau}^a(x) \dots, \\ \hat{\omega}_{\mu}^{AB}(x, \Theta) &= \omega_{\mu}^{AB}(x) - i\Theta^{\nu\rho}\omega_{\mu\nu\rho}^{AB}(x) + \Theta^{\nu\rho}\Theta^{\lambda\tau}\omega_{\mu\nu\rho\lambda\tau}^{AB}(x) \dots \end{aligned} \quad (12)$$

The tetrad fields  $\hat{e}_\mu^a(x, \Theta)$  result from the expansion of the non-commutative modifications applied to the gauge connection  $\hat{\omega}_\mu^{AB}(x, \Theta)$ , presented in Eq. (12), truncated to second-order terms in the parameter  $\Theta$

$$\omega_{\mu\nu\rho}^{AB}(x) = \frac{1}{4} \{\omega_\nu, \partial_\rho \omega_\mu + R_{\rho\mu}\}^{AB}, \quad (13a)$$

$$\begin{aligned} \omega_{\mu\nu\rho\lambda\tau}^{AB}(x) &= \frac{1}{32} (-\{\omega_\lambda, \partial_\tau \{\omega_\nu, \partial_\rho \omega_\mu + R_{\rho\mu}\}\} + 2\{\omega_\lambda, \{R_{\tau\nu}, R_{\mu\rho}\}\} \\ &\quad - \{\omega_\lambda, \{\omega_\nu, D_\rho R_{\tau\mu} + \partial_\rho R_{\tau\mu}\}\} - \{\{\omega_\nu, \partial_\rho \omega_\lambda + R_{\rho\lambda}\}, (\partial_\tau \omega_\mu + R_{\tau\mu})\}) \\ &\quad + 2[\partial_\nu \omega_\lambda, \partial_\rho (\partial_\tau \omega_\mu + R_{\tau\mu})]^{AB}. \end{aligned} \quad (13b)$$

Obtained through the application of the Seiberg–Witten map, Eqs. (13a) and (13b) obey to the following conditions:

$$[\alpha, \beta]^{AB} = \alpha^{AC} \beta_C^B - \beta^{AC} \alpha_C^B, \quad \{\alpha, \beta\}^{AB} = \alpha^{AC} \beta_C^B + \beta^{AC} \alpha_C^B, \quad (14)$$

and

$$D_\mu R_{\rho\sigma}^{AB} = \partial_\mu R_{\rho\sigma}^{AB} + (\omega_\mu^{AC} R_{\rho\sigma}^{DB} + \omega_\mu^{BC} R_{\rho\sigma}^{DA}) \eta_{CD}. \quad (15)$$

It is essential to emphasize certain constraints associated with the gauge connection  $\hat{\omega}_\mu^{AB}(x, \Theta)$ :

$$\hat{\omega}_\mu^{AB*}(x, \Theta) = -\hat{\omega}_\mu^{AB}(x, \Theta), \quad \hat{\omega}_\mu^{AB}(x, \Theta)^r \equiv \hat{\omega}_\mu^{AB}(x, -\Theta) = -\hat{\omega}_\mu^{BA}(x, \Theta), \quad (16)$$

The superscript  $*$  denotes the complex conjugate operation. Additionally, the non-commutative corrections arising from the constraints given in Eq. (16) can be formulated as

$$\omega_\mu^{AB}(x) = -\omega_\mu^{BA}(x), \quad \omega_{\mu\nu\rho}^{AB}(x) = \omega_{\mu\nu\rho}^{BA}(x), \quad \omega_{\mu\nu\rho\lambda\tau}^{AB}(x) = -\omega_{\mu\nu\rho\lambda\tau}^{BA}(x). \quad (17)$$

Above equations are derived by applying Eqs. (13a) and (13b) under the conditions of vanishing torsion field  $T_{\mu\nu}^a$  and the limit  $\mathcal{K} \rightarrow 0$ . For this expression, the complex conjugate of the deformed tetrad fields can be represented as

$$\hat{e}_\mu^{a*}(x, \Theta) = e_\mu^a(x) + i\Theta^{\nu\rho} e_{\mu\nu\rho}^a(x) + \Theta^{\nu\rho} \Theta^{\lambda\tau} e_{\mu\nu\rho\lambda\tau}^a(x) \dots, \quad (18)$$

in which

$$e_{\mu\nu\rho}^a = \frac{1}{4} [\omega_\nu^{ac} \partial_\rho e_\mu^d + (\partial_\rho \omega_\mu^{ac} + R_{\rho\mu}^{ac}) e_\nu^d] \eta_{ad}, \quad (19)$$



and

$$\begin{aligned}
e_{\mu\nu\rho\lambda\tau}^a(x) = & \frac{1}{32} \left[ 2 \{R_{\tau\nu}, R_{\mu\rho}\}^{ab} e_\lambda^c - \omega_\lambda^{ab} (D_\rho + \partial_\rho) R_{\tau\mu}^{cd} e_\nu^m \eta_{dm} \right. \\
& - \{\omega_\nu, (D_\rho + \partial_\rho) R_{\tau\mu}\}^{ab} e_\lambda^c - \partial_\tau \{\omega_\nu, (\partial_\rho \omega_\mu + R_{\rho\mu})\}^{ab} e_\lambda^c \\
& - \omega_\lambda^{ab} \partial_\tau (\omega_\nu^{cd} \partial_\rho e_\mu^m + (\partial_\rho \omega_\mu^{cd} + R_{\rho\mu}^{cd}) e_\nu^m) \eta_{dm} + 2 \partial_\nu \omega_\lambda^{ab} \partial_\rho \partial_\tau e_\mu^c \\
& - 2 \partial_\rho (\partial_\tau \omega_\mu^{ab} + R_{\tau\mu}^{ab}) \partial_\nu e_\lambda^c - \{\omega_\nu, (\partial_\rho \omega_\lambda + R_{\rho\lambda})\}^{ab} \partial_\tau e_\mu^c \\
& \left. - (\partial_\tau \omega_\mu^{ab} + R_{\tau\mu}^{ab}) (\omega_\nu^{cd} \partial_\rho e_\lambda^m + (\partial_\rho \omega_\lambda^{cd} + R_{\rho\lambda}^{cd}) e_\nu^m \eta_{dm}) \right] \eta_{bc}.
\end{aligned} \tag{20}$$

Consequently, the deformed metric tensor can be expressed as

$$g_{\mu\nu}^\Theta(x, \Theta) = \frac{1}{2} \eta_{ab} (\hat{e}_\mu^a(x, \Theta) * \hat{e}_\nu^{b*}(x, \Theta) + \hat{e}_\mu^b(x, \Theta) * \hat{e}_\nu^{a*}(x, \Theta)), \tag{21}$$

in which the symbol  $*$  represents the standard star product. For the remainder of the calculations, we shall adopt natural units, setting  $\hbar = c = G = 1$ . Thereby, we have

$$\begin{aligned}
g_{tt}^\Theta &= g_{tt} - \frac{\alpha(8r-11\alpha)}{16r^4} \Theta^2 + \mathcal{O}(\Theta^4), \\
g_{rr}^\Theta &= g_{rr} - \frac{\alpha(4r-3\alpha)}{16r^2(r-\alpha)^2} \Theta^2 + \mathcal{O}(\Theta^4), \\
g_{\theta\theta}^\Theta &= g_{\theta\theta} - \frac{2r^2-17\alpha r+17\alpha^2}{32r(r-\alpha)} \Theta^2 + \mathcal{O}(\Theta^4), \\
g_{\varphi\varphi}^\Theta &= g_{\varphi\varphi} - \frac{(r^2+\alpha r-\alpha^2) \cos\theta - \alpha(2r-\alpha)}{16r(r-\alpha)} \Theta^2 + \mathcal{O}(\Theta^4).
\end{aligned} \tag{22}$$

To determine the radius of the deformed Schwarzschild event horizon, the condition  $1/g_{rr}^\Theta = 0$  is imposed, i.e., up to the second order of  $\Theta$ , consistent with the method described in Ref. [12]. Applying this condition yields:

$$r_{s\Theta} = 2M - \frac{\Theta^2}{32M}. \tag{23}$$

The radius  $r_{s\Theta} = 2M_\Theta$  represents the modified event horizon associated with the deformed non-commutative mass of the Schwarzschild black hole. This correction introduces a redefined mass parameter expressed as [169, 170]:

$$M_\Theta = M - \frac{1}{64M} \Theta^2. \tag{24}$$

Throughout this analysis, the Schwarzschild metric is utilized, incorporating the corrected non-commutative mass defined in Eq. (24).

### III. A CORRECTED NEWMAN–JANIS TECHNIQUE

A widely utilized method for constructing rotating black hole solutions from spherically symmetric spacetimes is the Newman–Janis procedure [153, 154]. In this work, a mod-

ified approach called the non-complexification Newman–Janis algorithm [156, 157] is applied. This variation eliminates the complexification step, making it particularly effective for obtaining rotating metrics in systems involving imperfect fluids, starting from static, spherically symmetric configurations [158–163]. In our case, we consider

$$ds^2 = -f_{\Theta}(r)dt^2 + \frac{dr^2}{f_{\Theta}(r)} + r^2(d\theta^2 + \sin^2\theta d\varphi^2), \quad (25)$$

in which  $f_{\Theta}(r) \equiv 1 - 2M_{\Theta}/r$ .

The method begins by converting the metric into advanced null coordinates, specifically the Eddington–Finkelstein coordinates  $(u, r, \theta, \phi)$ . This is achieved through the coordinate transformation:

$$du = dt - \frac{dr}{f_{\Theta}(r)}, \quad (26)$$

which allows the static metric to be re-expressed as:

$$ds^2 = -f_{\Theta}(r)du^2 - 2dudr + r^2(d\theta^2 + \sin^2\theta d\phi^2). \quad (27)$$

A basis of null tetrad vectors is introduced, defined as  $Z_{\mu}^{\alpha} = (l_{\mu}, n_{\mu}, m_{\mu}, \bar{m}_{\mu})$ . The inverse metric tensor  $g^{\mu\nu}$  can then be expressed in terms of these vectors as

$$g^{\mu\nu} = -l^{\mu}n^{\nu} - l^{\nu}n^{\mu} + m^{\mu}\bar{m}^{\nu} + m^{\nu}\bar{m}^{\mu}. \quad (28)$$

The tetrad vector components are explicitly defined as

$$l^{\mu} = \delta_{\mu}^r, \quad n^{\mu} = \delta_{\mu}^u - \frac{1}{2}f_{\Theta}(r)\delta_{\mu}^r, \quad m^{\mu} = \frac{1}{\sqrt{2}r} \left( \delta_{\theta}^{\mu} + \frac{i}{\sin\theta} \delta_{\phi}^{\mu} \right). \quad (29)$$

Within this framework,  $\bar{m}_{\mu}$  represents the complex conjugate of  $m_{\mu}$ . The null tetrad vectors form an orthonormal basis and satisfy the following conditions  $l^{\mu}l_{\mu} = n^{\mu}n_{\mu} = m^{\mu}m_{\mu} = l^{\mu}m_{\mu} = n^{\mu}m_{\mu} = 0$ , and  $l^{\mu}n_{\mu} = -m^{\mu}\bar{m}_{\mu} = -1$ .

A complex coordinate transformation is then implemented, redefining  $\delta_{\mu}^{\nu}$  according to the following relation [155]

$$\delta_{\mu}^r \rightarrow \delta_{\mu}^r, \quad \delta_{\mu}^u \rightarrow \delta_{\mu}^u, \quad \delta_{\mu}^{\theta} \rightarrow \delta_{\mu}^r + ia \sin\theta(\delta_{\mu}^u - \delta_{\mu}^r), \quad \delta_{\mu}^{\phi} \rightarrow \delta_{\mu}^{\phi}. \quad (30)$$

In this formulation, the spin parameter of the black hole is denoted by  $a$ . The challenge of complexifying the radial coordinate is addressed using the modified Newman–Janis algorithm developed in [155, 171]. Rather than directly complexifying  $r$ , this method transforms the

radial function  $f(r)$  into a more general expression  $F(r, a, \theta)$  and replaces  $r^2$  with a redefined term  $H(r, a, \theta)$ . By following the steps detailed in [155, 171], the null tetrad vectors after this transformation are given by:

$$l'_\mu = \delta_r^\mu, \quad n'^\mu = \delta_u^\mu - F(r, a, \theta)\delta_r^\mu, \quad m'^\mu = \frac{1}{\sqrt{2H(r, a, \theta)}} [ia \sin \theta (\delta_u^\mu - \delta_r^\mu) + \delta_\theta^\mu + \sin \theta \delta_\phi^\mu], \quad (31)$$

With the necessary preliminaries established, the resulting expression is obtained below

$$g^{\mu\nu} = -l'^\mu n'^\nu - l'^\nu n'^\mu + m'^\mu \bar{m}'^\nu + m'^\nu \bar{m}'^\mu. \quad (32)$$

Following this method, a rotating black hole solution can be constructed in Eddington–Finkelstein coordinates, as presented as follows [171]

$$ds^2 = -F(r, a, \theta)du^2 - 2dudr + 2a \sin^2 \theta (F(r, a, \theta) - 1) dud\phi + 2a \sin^2 \theta drd\phi + H(r, a, \theta)d\theta^2 + \sin^2 \theta [H(r, a, \theta) + a^2 \sin^2 \theta (2 - F(r, a, \theta))] d\phi^2. \quad (33)$$

The function  $F(r, a, \theta)$  originates from the deformation of the radial component  $f_\Theta(r)$ . This modified approach provides a versatile framework applicable to generating rotating spacetimes from any spherically symmetric black hole solution [172–175]. To express the metric in Boyer–Lindquist coordinates, a global transformation is performed [171]:

$$du = dt' + \lambda(r)dr, \quad d\phi = d\phi' + \chi(r)dr. \quad (34)$$

The functions  $\lambda(r)$  and  $\chi(r)$  are entirely radial dependent and can be expressed as [171]:

$$\lambda(r) = -\frac{r^2 + a^2}{f_\Theta(r)(r^2 + a^2)}, \quad \chi(r) = -\frac{a}{f_\Theta(r)(r^2 + a^2)}. \quad (35)$$

To eliminate the cross-term  $dt'dr$  from the metric, the following condition is imposed:

$$F(r, a, \theta) = \frac{f_\Theta(r)r^2 + a^2 \cos^2 \theta}{H(r, a, \theta)}. \quad (36)$$

Additionally, the requirement for the Einstein tensor component  $G_{r\theta}$  to vanish leads to the constraint:

$$H(r, a, \theta) = r^2 + a^2 \cos^2 \theta. \quad (37)$$

These conditions, when applied and followed by a series of algebraic adjustments, yield the final expression for the rotating black hole metric in Boyer–Lindquist coordinates [155, 171]

$$ds^2 = \left[ \frac{\Delta(r) - a^2 \sin^2 \theta}{\Sigma} \right] dt^2 + \frac{\Sigma}{\Delta(r)} dr^2 + \Sigma d\theta^2 - 2a \sin^2 \theta \left[ 1 - \frac{\Delta(r) - a^2 \sin^2 \theta}{\Sigma} \right] dt d\phi + \frac{\sin^2 \theta}{\Sigma} [(r^2 + a^2)^2 - \Delta(r)a^2 \sin^2 \theta] d\phi^2, \quad (38)$$

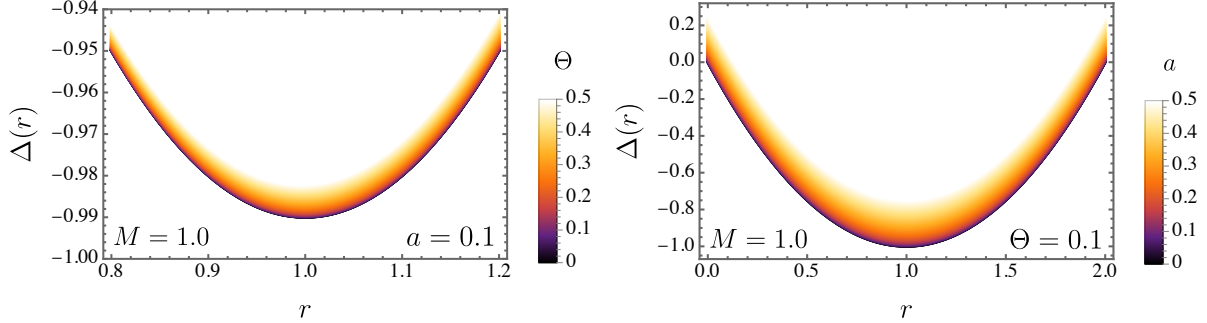


Figure 1: The parameter  $\Delta(r)$  is shown as a function of  $r$  for different combinations of  $\Theta$  and  $a$ .

in which  $\Delta(r) = a^2 + r^2 f_{\Theta}(r)$  and  $\Sigma = r^2 + a^2 \cos^2 \theta$ . These relations define the rotating modification of the static metric. Since  $\Delta(r)$  governs key geometric aspects of the black hole, its behavior is analyzed in Fig. 1, where it is plotted against the radial coordinate  $r$  for different values of the non-commutative parameter  $\Theta$  and the spin parameter  $a$ .

The subsequent sections will explore the fundamental properties and features of the derived rotating metric.

## IV. THE GENERAL REMARKS AND THERMAL BEHAVIOR

### A. The horizons and the corresponding ergospheres

This section focuses on examining both the thermodynamic properties of the metric in Eq. (38) and the geometric structures of the event horizon and ergosphere. To identify the physical horizons, the condition  $1/g_{rr} = 0$  is imposed, which simplifies to solving  $\Delta(r) = 0$

$$r_+ = \frac{\sqrt{(\Theta^2 - 64M^2)^2 - 4096a^2M^2 - \Theta^2 + 64M^2}}{64M}, \quad (39)$$

where  $r_+$  denotes the outer event horizon and

$$r_- = -\frac{\sqrt{(\Theta^2 - 64M^2)^2 - 4096a^2M^2 + \Theta^2 - 64M^2}}{64M}, \quad (40)$$

represents the inner horizon. As the parameter  $\Theta$  approaches zero, the expressions for both horizons reduce to those of the standard Kerr black hole. To illustrate the behavior of the outer event horizon more effectively, Fig. 2 provides a detailed visualization. The top left

panel shows the variation of  $r_+$  with the mass parameter  $M$  for different values of  $\Theta$ , keeping the spin parameter fixed at  $a = 0.5$ . In the top right panel, the dependence of  $r_+$  on  $M$  is plotted for varying spin parameter values while  $\Theta$  is held constant at 0.1. The bottom panel further explores this relation with a three-dimensional plot of  $r_+$  as a function of both  $a$  and  $\Theta$  with a fixed mass value of  $M = 2$ .

The analysis now moves to the ergosphere structure, defined by the condition  $g_{tt} = 0$ . Solving this equation, it leads to the following expression:

$$r_{e\pm} = \frac{\pm\sqrt{(\Theta^2 - 64M^2)^2 - 4096a^2M^2\cos^2(\theta)} - \Theta^2 + 64M^2}{64M}. \quad (41)$$

The ergosphere is characterized by the surfaces defined by  $r_{e\pm}$ , which depend on the spin parameter  $a$ , mass  $M$ , non-commutative parameter  $\Theta$ , and the angular coordinate  $\theta$ . As  $\Theta \rightarrow 0$ , this structure reduces to the familiar Kerr black hole ergosphere. The presence of the  $\cos(2\theta)$  term introduces angular dependence, causing the ergosphere to deviate from a perfect sphere, appearing flattened near the rotation axis at  $\theta = 0$  and  $\theta = \pi$ . The region lies between the two surfaces described by  $r_{e\pm}$ , where the temporal component of the metric,  $g_{tt}$ , becomes negative and behaves like a spatial coordinate. Consequently, any particle within this region must rotate in the same direction as the central mass to maintain a time-like trajectory, ensuring positive proper time as it moves through spacetime.

Fig. 3 illustrates the inner and outer ergosphere boundaries through a parametric plot for varying spin parameter values  $a$ , with the non-commutative parameter fixed at  $\Theta = 0.01$  and mass set to  $M = 1$ . A significant effect of non-commutativity, compared to the standard Kerr black hole, is the noticeable contraction of the ergosphere along the  $z$ -axis, resulting in a more compressed structure in that direction.

## B. The angular velocity

Analogous to the Kerr black hole, the presented solution displays symmetries related to time invariance and rotational symmetry, characterized by the existence of Killing vectors. The *Lense-Thirring* effect causes a stationary observer positioned outside the event horizon, with zero angular momentum relative to an observer at infinity, to be set into rotational motion. In the non-commutative black hole spacetime, this frame-dragging originates, among other factors, from the non-zero off-diagonal metric component  $g_{t\phi}$ . Therefore, the

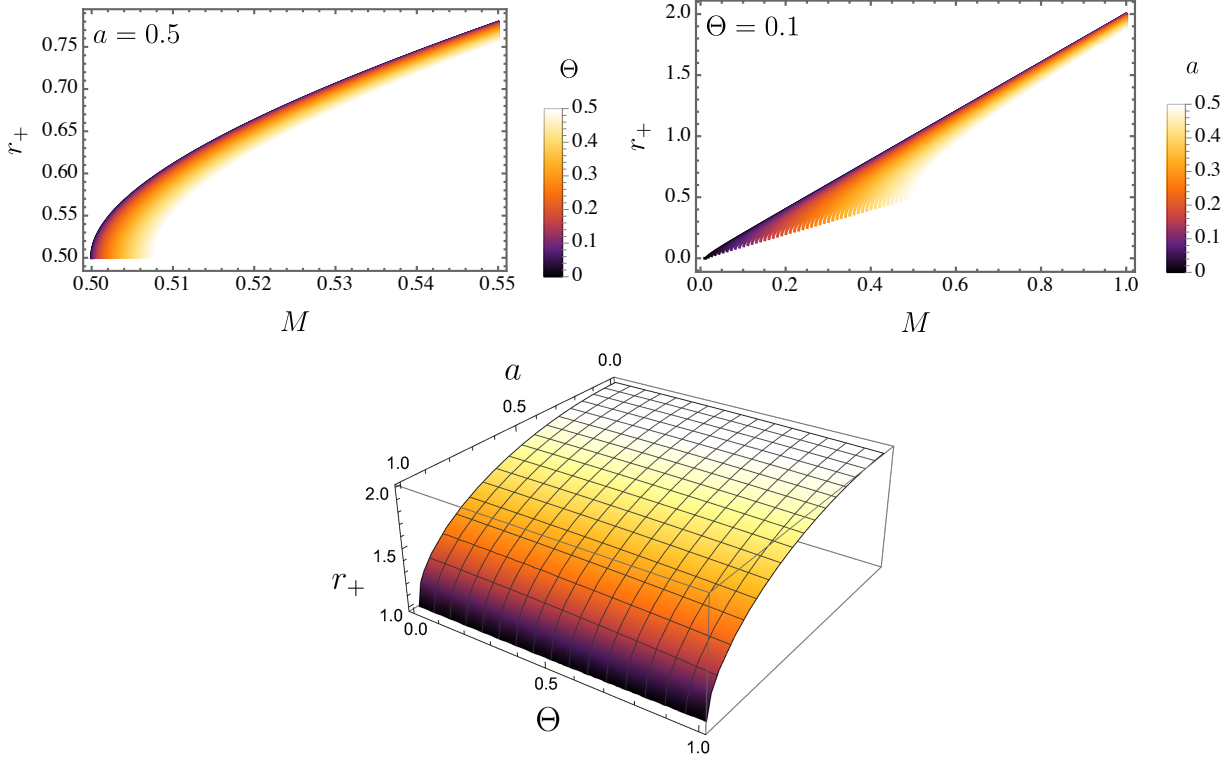


Figure 2: The top left panel displays the behavior of  $r_+$  as a function of the mass parameter  $M$  for various values of  $\Theta$  while keeping the spin parameter fixed at  $a = 0.5$ . The top right panel illustrates the dependence of  $r_+$  on  $M$  for different spin parameter values, with  $\Theta$  held constant at 0.1. The bottom panel presents a three-dimensional plot of  $r_+$  as a function of both  $a$  and  $\Theta$ , keeping the mass parameter fixed at  $M = 1$ .

observer's angular velocity is determined by [176, 177]

$$\begin{aligned}
 \omega(r) &= -\frac{g_{t\phi}}{g_{\phi\phi}} = \frac{a[a^2 + r^2 - \Delta(r)]}{(r^2 + a^2)^2 - a^2\Delta(r)\sin\theta} \\
 &= \frac{ar^2(32a^2M - r(\Theta^2 + 32M(r - 2M)))}{a^2\sin(\theta)(32a^2M(r^2 - 1) + r^2(\Theta^2(-r) - 32M(-2Mr + r^2 + 1))) + 32M(a^2 + r^2)^2}.
 \end{aligned} \tag{42}$$

As we can naturally expect, by setting the non-commutative parameter  $\Theta$  to zero, we recover the standard Kerr expression for the angular velocity. Fig. 4 depicts the angular velocity  $\omega$  for different values of the spin parameter  $a$  and the non-commutative parameter  $\Theta$ , highlighting the comparison with the classical Kerr case ( $\Theta = 0$ ). As  $\Theta$  increases,  $\omega(r)$  also tends to decrease, whereas larger values of  $a$  lead to an increase in the magnitude of  $\omega(r)$  (until  $r \approx 2$ ). Fig. 5 provides a three-dimensional representation of this behavior:

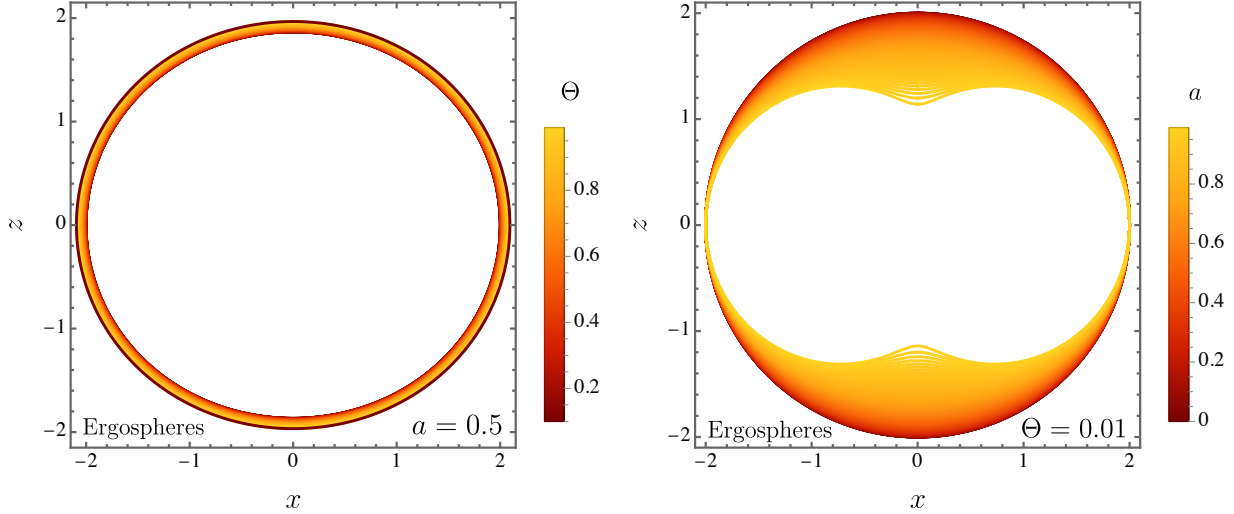


Figure 3: The parametric plot of the ergosphere is shown for different combinations of the non-commutative parameter  $\Theta$  and the spin parameter  $a$ .

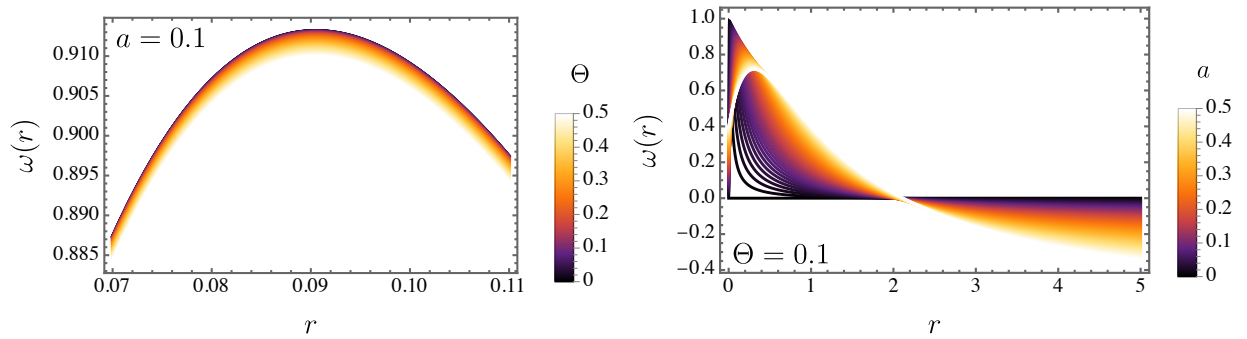


Figure 4: The angular velocity  $\omega$  is shown in two-dimensional plots for different values of the spin parameter  $a$  and the non-commutative parameter  $\Theta$ .

the left panel illustrates  $\omega(r)$  as a function of  $\Theta$  and  $r$ , while the right panel displays the dependence of the angular velocity on both  $a$  and  $r$ .

### C. The surface gravity

The calculation of the surface gravity involves a coordinate transformation from the form given in Eq. (38) to the Eddington–Finkelstein coordinates [178, 179], which remove the coordinate singularities occurring when  $\Delta(r) = 0$ . This transformation introduces modified

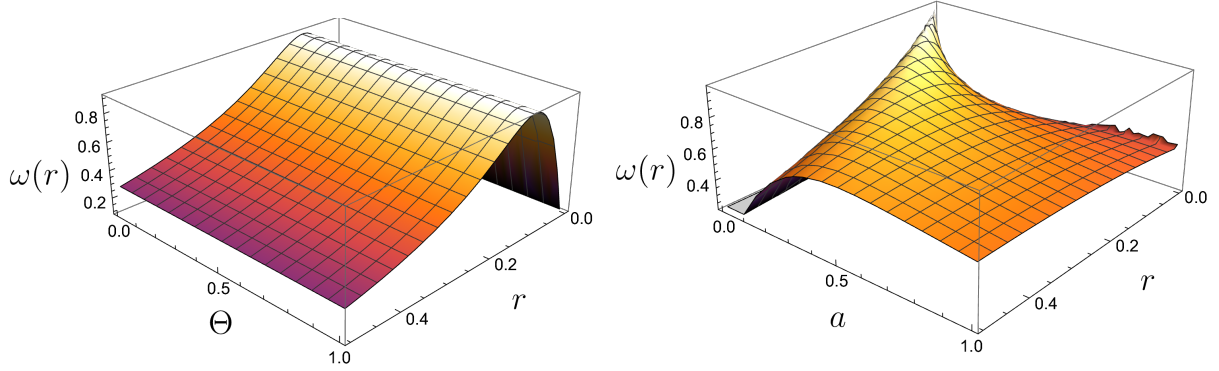


Figure 5: The angular velocity  $\omega$  is depicted using three-dimensional plots for various values of the spin parameter  $a$  and the non-commutative parameter  $\Theta$ .

time and angular coordinates,  $\tau$  and  $\chi$ , respectively, defined as follows:

$$d\tau = dt + \frac{r^2 + a^2}{\Delta(r)} dr, \quad (43)$$

and, also,

$$d\chi = d\varphi + \frac{a}{\Delta(r)} dr, \quad (44)$$

so that

$$ds^2 = \frac{\Delta(r) - a^2 \sin^2 \theta}{\Sigma} d\tau^2 + 2d\tau dr - \frac{2a(r^2 + a^2 - \Delta(r)) \sin^2 \theta}{\Sigma} d\tau d\chi - 2a \sin^2 \theta dr d\chi - \frac{(r^2 + a^2)^2 - \Delta(r) a^2 \sin^2 \theta}{\Sigma} d\chi^2. \quad (45)$$

By performing this change of variables, it turns out to be evident that on the hypersurfaces where  $r = r_{\pm}$ , the Killing vectors associated with the coordinates can be expressed as:

$$\psi_{\pm} = \frac{\partial}{\partial \tau} + \frac{\Delta(r)}{r_{\pm}^2 + a^2} \frac{\partial}{\partial \chi}. \quad (46)$$

Additionally, the Killing vectors can be rewritten using Boyer–Lindquist coordinates. Consider a Killing horizon  $K$ , defined by the normal Killing vector  $\xi$ . The surface gravity  $\kappa$  is described as the constant of proportionality between the vectors  $\xi^{\nu} \nabla_{\nu} \xi^{\mu}$  and  $\xi^{\mu}$  [180]. In this manner, we have

$$k_{+} = \frac{\Delta'(r_{+})}{2(r_{+}^2 + a^2)} = \frac{32M \sqrt{(\Theta^2 - 64M^2)^2 - 4096a^2M^2}}{(64M^2 - \Theta^2) \left( \sqrt{(\Theta^2 - 64M^2)^2 - 4096a^2M^2} - \Theta^2 + 64M^2 \right)}. \quad (47)$$

The surface gravity, as will be examined in the subsequent subsections, plays a fundamental role in the analysis of the thermodynamic properties associated with the black hole under study.



### D. The Hawking temperature

In 1973, the foundational principles of black hole mechanics were outlined by Bardeen, Carter, and Hawking, highlighting a close correspondence with the classical laws of thermodynamics [181]. The zeroth law asserts that surface gravity remains constant across the event horizon, resembling the uniform temperature of a system in thermal equilibrium [182]. The first law connects variations in a black hole's mass to changes in its surface area, angular momentum, and possibly electric charge, analogous to how internal energy shifts in thermodynamics relate to heat and work [183]. The second law establishes that the total area of the event horizon never decreases, reflecting the thermodynamic rule that entropy in an isolated system cannot decrease [184]. Lastly, the third law states that surface gravity cannot be reduced to zero through physical processes, mirroring the thermodynamic principle that absolute zero cannot be achieved [185].

The understanding of black hole mechanics was further developed through the contributions of Christodoulou, who investigated irreversible processes in black hole dynamics [186], and Bekenstein, who introduced the concept of black hole entropy. Bekenstein proposed that a black hole's entropy is directly proportional to the area of its event horizon [187, 188], leading to the formulation of the Bekenstein–Hawking entropy, which formally connects black hole mechanics to thermodynamic principles. Throughout this analysis, unless otherwise specified, all thermodynamic quantities will be evaluated under the assumption that  $\Theta, a < M$ . The expression for the Hawking temperature is given by:

$$T(\Theta, a, M) = \frac{k_+}{2\pi} = \frac{16M\sqrt{(\Theta^2 - 64M^2)^2 - 4096a^2M^2}}{\pi(64M^2 - \Theta^2)\left(\sqrt{(\Theta^2 - 64M^2)^2 - 4096a^2M^2} - \Theta^2 + 64M^2\right)}. \quad (48)$$

Fig. 6 illustrates how the thermodynamic quantity varies under the influence of the non-commutative parameter  $\Theta$  and the rotational parameter  $a$ . As shown in the left panel, an increase in  $\Theta$  results in a lower temperature magnitude (for small values of  $M$ ), while a similar effect is observed when  $a$  increases, further suppressing the temperature. To emphasize the impact of these modifications, the behavior is compared with the standard Kerr black hole, showing how the additional parameters alter the thermal properties of the system.

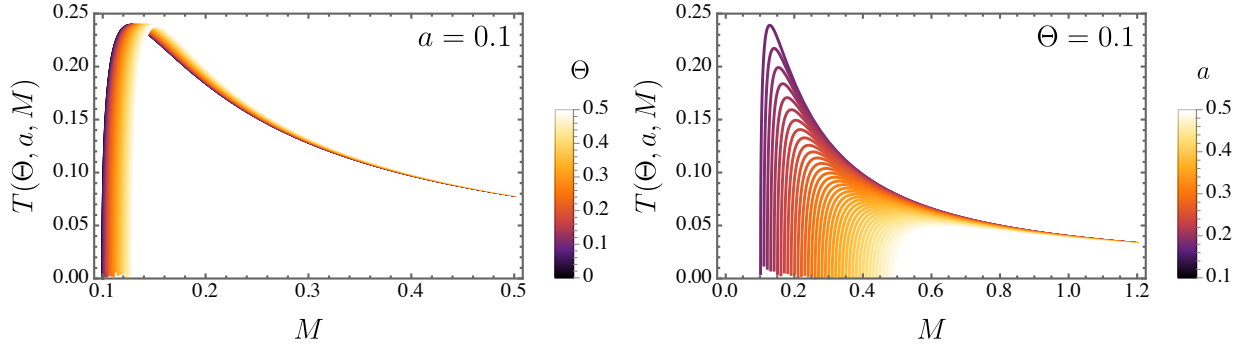


Figure 6: The behavior of the Hawking temperature is represented as a function of  $M$  for different choices of the non-commutative parameter  $\Theta$ , while keeping the rotational parameter fixed at  $a = 0.1$ .

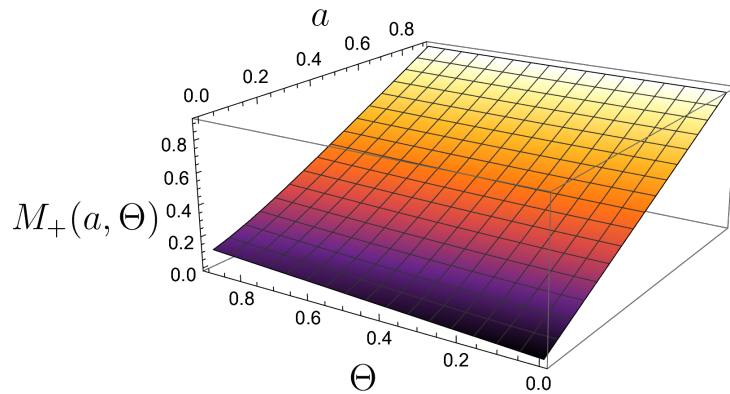


Figure 7: The remnant mass  $M_+(a, \Theta)$  is depicted in three-dimensional plots for different values of the spin parameter  $a$  and the non-commutative parameter  $\Theta$ .

### E. The remnant mass

By examining the extreme condition where the black hole reaches its final state, i.e.,  $T(\Theta, a, M) \rightarrow 0$ , the corresponding remnant mass is obtained

$$M_{\pm}(a, \Theta) = \frac{1}{8} \left( \sqrt{16a^2 + \Theta^2} \pm 4a \right). \quad (49)$$

As expected, this parameter depends on  $\Theta$  and  $a$ . Additionally, in the limit  $\Theta \rightarrow 0$ , the remnant mass of the Kerr black hole is recovered. Fig. 7 presents a three-dimensional plot of the remnant mass  $M_+(a, \Theta)$  for different values of  $a$  and  $\Theta$ .

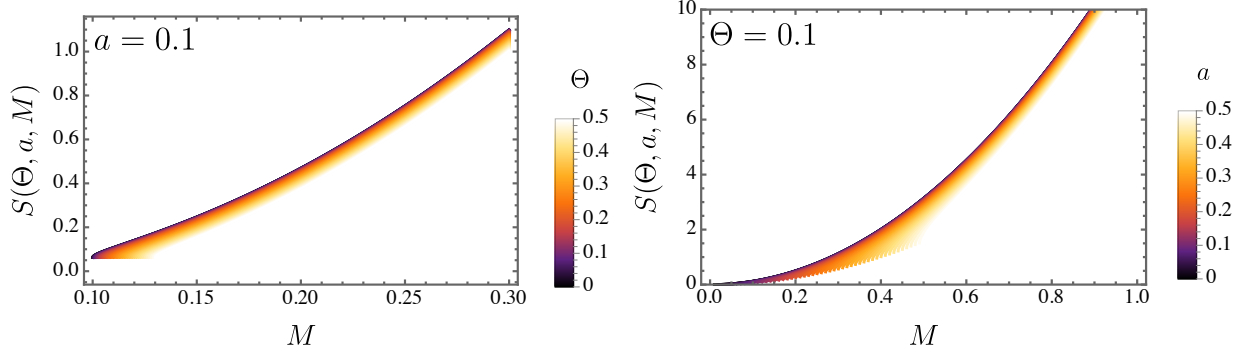


Figure 8: The entropy is shown as a function of  $M$  for different values of the non-commutative parameter  $\Theta$ , with the rotational parameter fixed at  $a = 0.1$ .

### F. The entropy

The expression for entropy is directly given by:

$$\begin{aligned}
 S(\Theta, a, M) &= \pi(r_+^2 + a^2) \\
 &= \pi \left( \frac{\left( \sqrt{(\Theta^2 - 64M^2)^2 - 4096a^2M^2} - \Theta^2 + 64M^2 \right)^2}{4096M^2} + a^2 \right). \tag{50}
 \end{aligned}$$

Fig. 8 illustrates the entropy behavior for a fixed rotational parameter  $a = 0.1$ , showing the influence of the non-commutative parameter  $\Theta$ . To highlight the modifications introduced by  $\Theta$ , the results are compared with the standard Kerr black hole ( $\Theta = 0$ ), revealing how the entropy is altered in the presence of non-commutativity. In general, an increase in both  $\Theta$  and  $a$  leads to a reduction in the magnitude of  $S(\Theta, a, M)$ .

### G. Heat capacity

To ensure a comprehensive analysis, the heat capacity is also examined. Its expression is given by:

$$\begin{aligned}
 C_V(\Theta, a, M) &= T \frac{\partial S}{\partial T} = T \frac{\partial S / \partial M}{\partial T / \partial M} \\
 &= \frac{\pi \Xi^3 (\Theta^2 - 64M^2) \sqrt{(\Theta^2 - 64M^2)^2 - 4096a^2M^2}}{2048M^2 \left( \Xi (\Theta^2 - 64M^2)^2 - 4096a^2M^2 \left( \sqrt{(\Theta^2 - 64M^2)^2 - 4096a^2M^2} - 2\Theta^2 + 128M^2 \right) \right)}, \tag{51}
 \end{aligned}$$

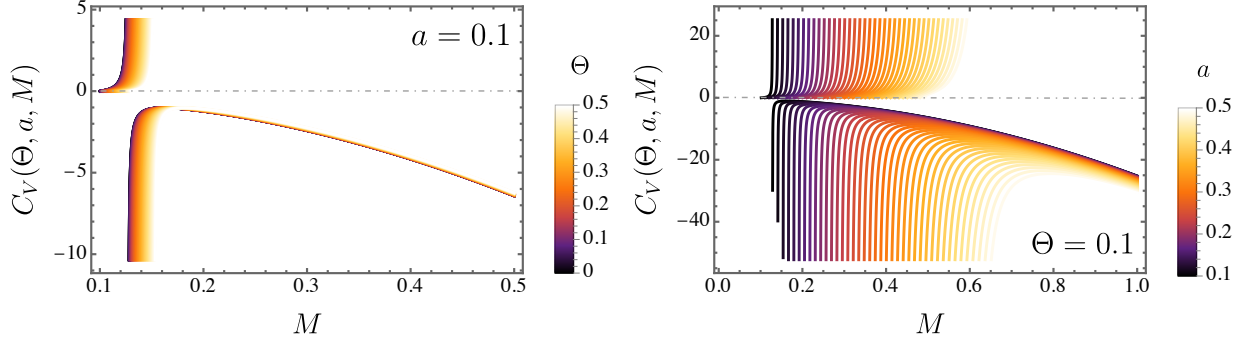


Figure 9: The heat capacity is represented as a function of  $M$ , considering different choices of the non-commutative parameter  $\Theta$  and the rotational parameter  $a$ .

in which

$$\Xi = \sqrt{(\Theta^2 - 64M^2)^2 - 4096a^2M^2 - \Theta^2 + 64M^2}. \quad (52)$$

Fig. 9 displays the behavior of the heat capacity for different values of the non-commutative parameter  $\Theta$ , with the rotational parameter held constant at  $a = 0.1$ . To emphasize the effects introduced by non-commutativity, the results are compared with the standard Kerr black hole, analogous to the previous thermodynamic functions. Furthermore, non-commutative gravity has been widely explored in various scenarios, including modifications of general relativity [189], scalar field models, Reissner–Nordström black holes [190–192], and BTZ black holes [193].

Finally, in Tab. I, we present the black hole parameters that are compared with those of another recently proposed axisymmetric black hole in the literature [10]. In addition,  $\hat{\xi} \equiv \pi^{3/4}M\sqrt{\sqrt{\pi}(M^2 - a^2) - 8\sqrt{\Theta}M} - 4\sqrt{\pi}\sqrt{\Theta}\sqrt{\sqrt{\pi}(M^2 - a^2) - 8\sqrt{\Theta}M} + 8\Theta + \pi M^2 - 8\sqrt{\pi}\sqrt{\Theta}M$  [10]. Furthermore, to avoid repeating the lengthy definitions of  $\Gamma$  and  $\tilde{\Gamma}$  in this manuscript, readers are referred to Ref. [10] for their explicit forms.

## V. HAWKING RADIATION AS A TUNNELING PROCESS

### A. Bosonic particle modes

To investigate the tunneling of massless particles from a rotating black hole, we adopt a metric where the worldlines describe photons with energy  $\omega$  propagating at infinity with constant  $\theta$ , and with the angular momentum component projected along the black hole’s

Table I: The black hole parameters are compared with those of another recently proposed axisymmetric black hole in the literature [10].

Parameters	This work	Lorentzian NC black hole [10]
$\Delta(r)$	$a^2 + r^2 \left[ 1 - \frac{2 \left( M - \frac{\Theta^2}{64M} \right)}{r} \right]$	$a^2 + r^2 \left[ \frac{8\sqrt{\Theta}M}{\sqrt{\pi r^2}} - \frac{2M}{r} + 1 \right]$
$r_{e\pm}$	$\pm \sqrt{\frac{(\Theta^2 - 64M^2)^2 - 4096a^2M^2 - \Theta^2 + 64M^2}{64M}}$	$\pm \frac{\sqrt{(3\Theta^2 + 64M^2)^2 - 4096a^2M^2 + 3\Theta^2 + 64M^2}}{64M}$
$r_{e+}$	$\pm \sqrt{\frac{(\Theta^2 - 64M^2)^2 - 4096a^2M^2 \cos^2(\theta) - \Theta^2 + 64M^2}{64M}}$	$\pm \frac{\sqrt{2} \sqrt{-\pi a^2 \cos(2\theta) - \pi a^2 + 2\pi M^2 - 16\sqrt{\pi} \sqrt{\Theta} M + 2\sqrt{\pi} M}}{2\sqrt{\pi}}$
$\omega(r)$	$\frac{ar^2 (32a^2M - r(\Theta^2 + 32M(r-2M)))}{a^2 \sin(\theta) (32a^2M(r^2 - 1) + r^2(\Theta^2 - r) - 32M(-2Mr + r^2 + 1)) + 32M(a^2 + r^2)^2}$	$\frac{2aM(\sqrt{\pi r} - 4\sqrt{\Theta})}{\sqrt{\pi}(a^2 + r^2)^2 - a^2 \sin(\theta)(\sqrt{\pi}(a^2 + r(2M)) + 8\sqrt{\Theta}M)}$
$k_+$	$\frac{32M \sqrt{(\Theta^2 - 64M^2)^2 - 4096a^2M^2}}{(64M^2 - \Theta^2) \left( \sqrt{(\Theta^2 - 64M^2)^2 - 4096a^2M^2} - \Theta^2 + 64M^2 \right)}$	$\frac{\sqrt{M \left( M - \frac{8\sqrt{\Theta}}{\sqrt{\pi}} \right) - a^2}}{\left( \sqrt{M \left( M - \frac{8\sqrt{\Theta}}{\sqrt{\pi}} \right) - a^2} + M \right)^2 + a^2}$
$T(\Theta, a, M)$	$\frac{16M \sqrt{(\Theta^2 - 64M^2)^2 - 4096a^2M^2}}{\pi(64M^2 - \Theta^2) \left( \sqrt{(\Theta^2 - 64M^2)^2 - 4096a^2M^2} - \Theta^2 + 64M^2 \right)}$	$\frac{\sqrt{M \left( M - \frac{8\sqrt{\Theta}}{\sqrt{\pi}} \right) - a^2}}{2\pi \left( \left( \sqrt{M \left( M - \frac{8\sqrt{\Theta}}{\sqrt{\pi}} \right) - a^2} + M \right)^2 + a^2 \right)}$
$S(\Theta, a, M)$	$\pi \left( \frac{\left( \sqrt{(\Theta^2 - 64M^2)^2 - 4096a^2M^2} - \Theta^2 + 64M^2 \right)^2}{4096M^2} + a^2 \right)$	$\frac{2\sqrt{M^2(2\xi - \pi a^2)}}{\sqrt{\pi}}$
$C_V(\Theta, a, M)$	$\frac{\pi \Xi^3 (\Theta^2 - 64M^2) \sqrt{(\Theta^2 - 64M^2)^2 - 4096a^2M^2}}{2048M^2 (\Xi(\Theta^2 - 64M^2)^2 - 4096a^2M^2) \left( \sqrt{(\Theta^2 - 64M^2)^2 - 4096a^2M^2} - 2\Theta^2 + 128M^2 \right)}$	$-\frac{\Gamma}{\Gamma}$

rotation axis given by  $L_z = a\omega \sin^2 \theta$ . These coordinates, referred to as the *Kerr ingoing coordinates* [148, 194], are derived through the transformation

$$dv = dt + \frac{(r^2 + a^2)}{\Delta(r)} dr, \quad d\phi = d\tilde{\phi} + \frac{a}{\Delta(r)} dr. \quad (53)$$

Additionally, the line element described in Eq. (38) takes the form

$$\begin{aligned} ds^2 = & - \left(1 - \frac{2M_{\Theta} r}{\Sigma}\right) dv^2 + 2dv dr + \Sigma d\theta^2 - \frac{4aM_{\Theta} r \sin^2 \theta}{\Sigma} d\phi dv \\ & - 2a \sin^2 \theta d\phi dr + \frac{(r^2 + a^2)^2 - a^2 \Delta(r) \sin^2 \theta}{\Sigma} \sin^2 \theta d\phi^2. \end{aligned} \quad (54)$$

In rotating black hole spacetimes, the *static limit surface*  $r_{\text{st}}$ , defined by the condition  $g_{tt} = 0$ , represents the outer boundary of the ergosphere and does not coincide with the event horizon. The applicability of the semiclassical approach in this scenario has been debated [195–206], as the geometric optics approximation remains more accurate near  $r_{\text{st}}$  than at the event horizon, where tunneling processes are typically analyzed. To address this issue, some works [195, 207] have implemented a co-rotating coordinate transformation,  $\phi \rightarrow \phi - \Omega^H t$ , where  $\Omega^H = a/(r_+^2 + a^2)$  denotes the angular velocity at the event horizon. However, it will be demonstrated that such a transformation is unnecessary, as the standard formulation already yields the correct result.

The semiclassical approach relies on the classical action  $I$  to determine the transition probability across the event horizon, governed by the relativistic Hamilton–Jacobi equation. Given that the metric in Eq. (54) does not explicitly depend on the coordinates  $v$  and  $\phi$ , the action can be expressed in the form  $I = -\omega v + J\phi + \mathcal{F}(\theta, r)$ . It will be shown that the imaginary contribution arises from the  $r$ -dependent component, which generates a pole at the horizon. Substituting this expression for  $I$  into the Hamilton–Jacobi equation leads to the following result

$$\begin{aligned} a^2(m \csc \theta - \omega \sin \theta)^2 + 2[a^2 m - (a^2 + r^2)\omega] \mathcal{F}_r + \\ + [a^2 + r(-2m + r)] \mathcal{F}_r^2 + \mathcal{F}_\theta^2 = 0, \end{aligned} \quad (55)$$

where the subscripts  $r$  and  $\theta$  denote partial derivatives with respect to  $r$  and  $\theta$ , respectively. When solving for  $\mathcal{F}_r(\theta, r)$ , it becomes evident that the integrand also depends on the coordinate  $\theta$ :

$$\mathcal{F}_r(\theta, r) = -\frac{X(r)}{\Delta(r)} \pm \frac{\sqrt{X(r)^2 - \Delta(r) [a^2(M_{\Theta} \csc \theta - \omega \sin \theta)^2 + \mathcal{F}_\theta(\theta, r)^2]}}{\Delta(r)} \quad (56)$$

where  $X(r) \equiv a^2 M_\Theta - (a^2 + r^2)\omega$ . A straightforward approach to address the  $\theta$  dependence is to set  $\theta = \theta_0$  as a constant and verify that the final expression does not depend on this choice [208]. However, this step can be avoided since the tunneling process is examined near the event horizon, where  $\Delta(r_+) = 0$ . In this regime, the  $\theta$ -dependent contribution vanishes, reducing the expression to a function of  $r$  alone. This simplification arises from the complete separability of the Hamilton–Jacobi equation in Kerr spacetime. Expressing all terms in relation to  $r_+$  and  $r_-$ , the expression for  $X(r)$  becomes  $X(r) = \frac{(r_+ + r_-)a^2}{2} - \omega(r_+^2 + a^2)$ , leading to

$$\text{Im } \mathcal{F}(\theta, r) = -\text{Im} \int dr \frac{X(r) + \sqrt{X^2(r) - (r - r_+)(r - r_-)} (\dots)}{(r - r_-)(r - r_+)} \quad (57)$$

where  $(\dots)$  represents all terms involving the  $\theta$  dependence. Applying Feynman’s prescription to regularize the integral,

$$\text{Im } I = -2\pi \frac{X(r_+)}{r_+ - r_-} = \pi \left[ 2\omega \frac{(r_+^2 + a^2)}{(r_+ - r_-)} - \frac{a^2(r_+ + r_-)}{(r_+ - r_-)} \right]. \quad (58)$$

By expressing  $J$  as  $J = \frac{a(r_+ + r_-)}{2}$  and incorporating the horizon’s angular velocity  $\Omega^H$ , the terms can be reorganized, resulting in the final form of the tunneling probability rate

$$\bar{\Gamma} = \exp[-2 \text{Im } I] = \exp[-\beta(\omega - \Omega^H J)], \quad (59)$$

where the inverse temperature is given by  $\beta = \frac{4\pi(r_+^2 + a^2)}{r_+ - r_-}$ . In the special case where both  $a \rightarrow 0$  and  $\Theta \rightarrow 0$ , the expression reduces to the well-known result for the Schwarzschild black hole. Moreover, the particle density for bosons can be expressed as

$$n_b(\omega, \Theta, a, M) = \frac{\bar{\Gamma}}{1 - \bar{\Gamma}} = \frac{1}{\exp\left(\frac{\pi(64M^2 - \Theta^2)\left(\omega\left(\sqrt{(\Theta^2 - 64M^2)^2 - 4096a^2M^2 - \Theta^2 + 64M^2}\right) - 32a^2M\right)}{16M\sqrt{(\Theta^2 - 64M^2)^2 - 4096a^2M^2}}\right) - 1}. \quad (60)$$

In Fig. 10, the bosonic particle creation rate,  $n_b(\omega, \Theta, a, M)$ , is plotted as a function of the frequency  $\omega$ . The left panel displays how different values of the non-commutative parameter  $\Theta$  affect the rate, whereas the right panel highlights the impact of varying the rotational parameter  $a$ . In general lines, for a fixed rotational parameter at  $a = 0.1$ , an increase in the non-commutative parameter  $\Theta$  results in an increment in the magnitude of the particle density. Conversely, when  $\Theta$  remains constant ( $\Theta = 0.1$ ), varying the rotational parameter  $a$  leads to an increase in  $n_b(\omega, \Theta, a, M)$ .

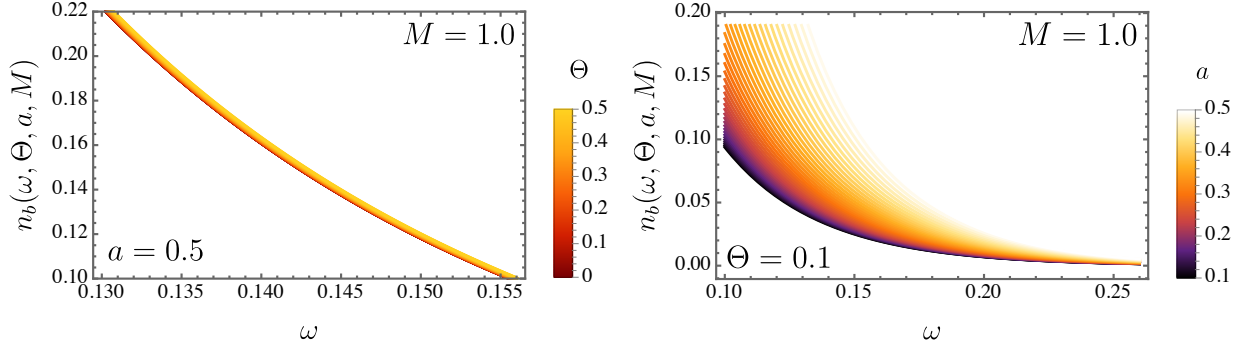


Figure 10: The particle creation rate for bosons, denoted by  $n_b(\omega, \Theta, a, M)$ , is represented as a function of the frequency  $\omega$ . The left panel illustrates the effect of varying the non-commutative parameter  $\Theta$ , while the right panel shows the influence of the rotational parameter  $a$ .

### B. Fermionic particle modes

The emission of Dirac particles through the tunneling formalism is now investigated at the outer event horizon of a Kerr black hole. For simplicity, the focus is restricted to a massless spinor field  $\Psi$  governed by the covariant Dirac equation

$$-i\hbar\gamma^a e_a^\mu \nabla_\mu \Psi = 0, \quad (61)$$

where  $\nabla_\mu$  represents the spinor covariant derivative, expressed as  $\nabla_\mu = \partial_\mu + \frac{1}{4}\omega_\mu^{ab}\gamma_{[a}\gamma_{b]}$ . Here,  $\omega_\mu^{ab}$  denotes the spin connection, which can be written in terms of the tetrad components  $e_a^\mu$ . The  $\gamma$  matrices are defined as

$$\gamma^0 = \begin{pmatrix} i & 0 \\ 0 & -i \end{pmatrix}, \gamma^1 = \begin{pmatrix} 0 & \sigma^3 \\ \sigma^3 & 0 \end{pmatrix}, \gamma^2 = \begin{pmatrix} 0 & \sigma^1 \\ \sigma^1 & 0 \end{pmatrix}, \gamma^3 = \begin{pmatrix} 0 & \sigma^2 \\ \sigma^2 & 0 \end{pmatrix}, \quad (62)$$

where the matrices  $\sigma^k$  ( $k = 1, 2, 3$ ) represent the Pauli matrices and the tetrad fields  $e_a^\mu$  can be chosen as

$$e_0^\mu = \left( \sqrt{-g^{tt}}, 0, 0, \frac{-g^{t\phi}}{\sqrt{-g^{tt}}} \right), \quad e_1^\mu = \left( 0, \sqrt{\frac{\Delta(r)}{\Sigma}}, 0, 0 \right),$$

$$e_2^\mu = \left( 0, 0, \frac{1}{\sqrt{\Sigma}}, 0 \right), \quad e_3^\mu = \left( 0, 0, 0, \frac{1}{\sqrt{g_{\phi\phi}}} \right).$$



The spin-up spinor field  $\Psi$  is assumed using the following ansatz [209, 210]:

$$\Psi = \begin{pmatrix} A(t, r, \theta, \phi) \\ 0 \\ B(t, r, \theta, \phi) \\ 0 \end{pmatrix} \exp \left[ \frac{i}{\hbar} I(t, r, \theta, \phi) \right]. \quad (63)$$

The focus will be restricted to the spin-up case, as the spin-down scenario can be treated in an analogous manner. To implement the WKB approximation, the assumed form of the spinor field  $\Psi$  is substituted into the covariant Dirac equation. By isolating the exponential term and omitting terms proportional to  $\hbar$ , the resulting system simplifies to the following four equations

$$\begin{cases} iA \left( \sqrt{-g^{tt}} \partial_t I - \frac{g^{t\phi}}{\sqrt{-g^{tt}}} \partial_\phi I \right) + B \sqrt{\frac{\Delta}{\Sigma}} \partial_r I = 0, \\ \left( \frac{1}{\sqrt{\Sigma}} \partial_\theta I + i \frac{1}{\sqrt{g_{\phi\phi}}} \partial_\phi I \right) B = 0, \\ A \sqrt{\frac{\Delta}{\Sigma}} \partial_r I - iB \left( \sqrt{-g^{tt}} \partial_t I - \frac{g^{t\phi}}{\sqrt{-g^{tt}}} \partial_\phi I \right) = 0, \\ \left( \frac{1}{\sqrt{\Sigma}} \partial_\theta I + i \frac{1}{\sqrt{g_{\phi\phi}}} \partial_\phi I \right) A = 0. \end{cases} \quad (64)$$

It should be emphasized that while  $A$  and  $B$  vary, their derivatives, as well as the components  $\omega_\mu$ , are proportional to  $\hbar$  and can be disregarded in the leading-order WKB approximation. As the analysis is confined to the region outside the event horizon, the condition  $\Delta \geq 0$  holds throughout the equations derived above. Moreover, the second and fourth equations imply that

$$\frac{1}{\sqrt{\Sigma}} \partial_\theta I + i \frac{1}{\sqrt{g_{\phi\phi}}} \partial_\phi I = 0. \quad (65)$$

The first and third equations reveal that a non-trivial solution for  $A$  and  $B$  can only arise when the determinant of the coefficient matrix vanishes. This requirement results in the following expression

$$\left( \sqrt{-g^{tt}} \partial_t I - \frac{g^{t\phi}}{\sqrt{-g^{tt}}} \partial_\phi I \right)^2 - \frac{\Delta}{\Sigma} (\partial_r I)^2 = 0. \quad (66)$$

Since the Kerr spacetime possesses two Killing vectors,  $(\partial/\partial t)^\mu$  and  $(\partial/\partial \phi)^\mu$ , the classical action  $I(t, r, \theta, \phi)$  can be decomposed into separable variables

$$I = -\omega t + J\phi + R(r, \theta) + K, \quad (67)$$

where  $\omega$  denotes the energy and  $J$  the angular momentum of the Dirac particle, with  $K$  being a complex-valued constant. In this manner,

$$\left( \sqrt{-g^{tt}}\omega + \frac{g^{t\phi}}{\sqrt{-g^{tt}}}J \right)^2 - \frac{\Delta}{\Sigma}(\partial_r R)^2 = 0. \quad (68)$$

Observe that  $R(r, \theta)$  is a complex-valued function. By specifying a particular value of  $\theta_0$ , the expression becomes [207, 208]

$$\begin{aligned} R_{\pm}(r, \theta_0) &= \pm \int dr \sqrt{\frac{\Sigma(\theta_0)}{\Delta}} \left[ \sqrt{-g^{tt}(\theta_0)}\omega + \frac{g^{t\phi}(\theta_0)}{\sqrt{-g^{tt}(\theta_0)}}J \right], \\ &= \pm \int \frac{dr}{\Delta} \left[ \omega \sqrt{(r^2 + a^2)^2 - \Delta a^2 \sin^2 \theta_0} - J \frac{a(r^2 + a^2 - \Delta)}{\sqrt{(r^2 + a^2)^2 - \Delta a^2 \sin^2 \theta_0}} \right]. \end{aligned}$$

The imaginary part of  $R_+$  can be obtained from the expression above. By integrating around the pole near the event horizon, the following result is derived<sup>1</sup>

$$\text{Im}R_{\pm} = \pm \frac{\pi(r^2 + a^2)}{r_+ - r_-}(\omega - J\Omega^H), \quad (69)$$

where  $\Omega_H = \frac{a}{r_+^2 + a^2}$  represents the angular velocity at the event horizon. Notably, this expression shows no dependence on the coordinate  $\theta$ .

According to the Hamilton–Jacobi method [211, 212], one solution describes Dirac particles escaping from the outer event horizon, while the other corresponds to particles approaching it. The probabilities for the particles crossing the outer horizon in both directions are expressed as

$$\begin{aligned} \mathcal{P}_{out} &= \exp \left[ -\frac{2}{\hbar} \text{Im}I \right] = \exp \left[ -\frac{2}{\hbar} (\text{Im}R_+ + \text{Im}K) \right], \\ \mathcal{P}_{in} &= \exp \left[ -\frac{2}{\hbar} \text{Im}I \right] = \exp \left[ -\frac{2}{\hbar} (\text{Im}R_- + \text{Im}K) \right]. \end{aligned} \quad (70)$$

To ensure that the probabilities are properly normalized, it is important to recognize that the likelihood of any incoming wave crossing the outer event horizon is equal to unity [211]. This condition establishes the relation  $\text{Im}K = -\text{Im}R_-$ . Furthermore, since  $\text{Im}R_+ = -\text{Im}R_-$ , the tunneling probability for a Dirac particle moving from inside to outside the event horizon reads

$$\begin{aligned} \hat{\Gamma} &= \exp \left[ -\frac{4}{\hbar} \text{Im}R_+ \right], \\ &= \exp \left[ \frac{4\pi(r_+^2 + a^2)}{(r_+ - r_-)}(\omega - J\Omega^H) \right]. \end{aligned} \quad (71)$$

---

<sup>1</sup> For a more detailed treatment, please, see [208, 211] and the references therein.

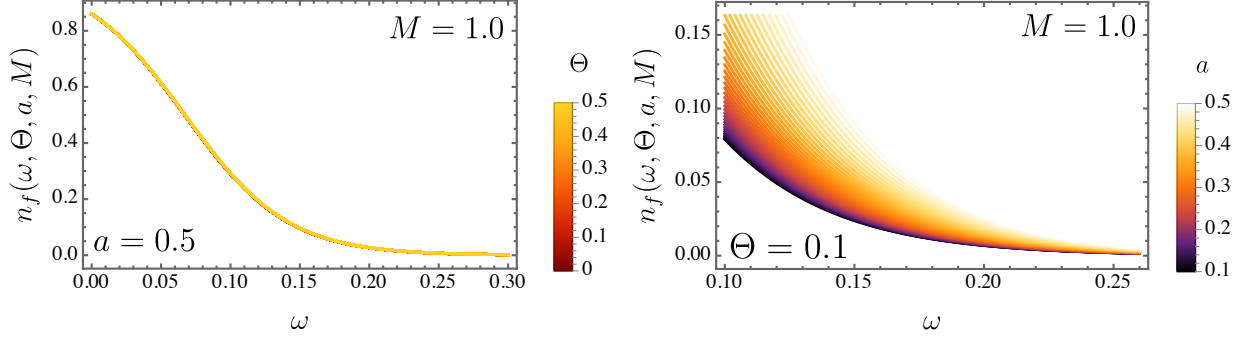


Figure 11: The particle creation rate for bosons, denoted by  $n_f(\omega, \Theta, a, M)$ , is represented as a function of the frequency  $\omega$ . The left panel illustrates the effect of varying the non-commutative parameter  $\Theta$ , while the right panel shows the influence of the rotational parameter  $a$ .

The fermionic spectrum of Hawking radiation for Dirac particles emitted from a Kerr black hole can be derived from the tunneling probability by applying standard methods of Refs. [213, 214]

$$\begin{aligned}
 n_f(\omega, \Theta, a, M) &= \frac{1}{e^{2\pi(\omega - J\Omega^H)/\kappa} + 1} \\
 &= \frac{1}{\exp\left(\frac{\pi(64M^2 - \Theta^2)\left(\omega\left(\sqrt{(\Theta^2 - 64M^2)^2 - 4096a^2M^2 - \Theta^2 + 64M^2} - 32a^2M\right)\right)}{16M\sqrt{(\Theta^2 - 64M^2)^2 - 4096a^2M^2}}\right) + 1}.
 \end{aligned} \tag{72}$$

Furthermore, in Fig. 11, the fermionic particle creation rate,  $n_f(\omega, \Theta, a, M)$ , is plotted as a function of the frequency  $\omega$ . The left panel displays how different values of the non-commutative parameter  $\Theta$  affect the rate, whereas the right panel highlights the impact of varying the rotational parameter  $a$ . In general lines, for a fixed rotational parameter at  $a = 0.1$ , an increase in the non-commutative parameter  $\Theta$  results in an increase of the particle density. Conversely, when  $\Theta$  remains constant, varying the rotational parameter  $a$  leads to an increase in  $n_f(\Theta, a, M)$ .

## VI. GEODESICS

This section investigates how non-commutativity affects the trajectories of particles moving along geodesics in the spacetime of a rotating black hole. The metric's axisymmetry, characterized by the Killing vectors  $\partial_t$  and  $\partial_\phi$ , allows the focus to be narrowed to radial motion, simplifying the analysis. The equations describing the particle dynamics along these

geodesics are derived from the Lagrangian formulation, following the methodology presented in [215], which serves as the framework for this analysis

$$\mathcal{L} = g_{\mu\nu} \dot{x}^\mu \dot{x}^\nu. \quad (73)$$

The parameter  $\mathcal{L}$  can be set to  $-1$ ,  $0$ , or  $1$ , representing timelike, null, and spacelike geodesics, respectively. The dot notation signifies differentiation with respect to the affine parameter  $\lambda$ , with the velocity components defined as  $\dot{x}^\mu = \frac{dx^\mu}{d\lambda}$ . Using this definition, the equations describing the particle motion take the following form

$$\begin{aligned} \mathcal{L} = & - \left[ \frac{\Delta(r) - a^2 \sin^2 \theta}{\Sigma} \right] \dot{t}^2 + \frac{\Sigma}{\Delta(r)} \dot{r}^2 + \Sigma \dot{\theta}^2 \\ & - 2a \sin^2 \theta \left[ 1 - \frac{\Delta(r) - a^2 \sin^2 \theta}{\Sigma} \right] \dot{t} \dot{\phi} + \frac{\sin^2 \theta}{\Sigma} [(r^2 + a^2)^2 - \Delta a^2 \sin^2 \theta] \dot{\phi}^2 \end{aligned} \quad (74)$$

To simplify the analysis, we confine the particle motion to the equatorial plane by fixing  $\theta = \frac{\pi}{2}$ . Under this condition, the previous equation simplifies to

$$\begin{aligned} \mathcal{L} = & - \left[ \frac{\Delta(r) - a^2}{\Sigma} \right] \dot{t}^2 + \frac{\Sigma}{\Delta(r)} \dot{r}^2 \\ & - 2a \left[ 1 - \frac{\Delta(r) - a^2}{\Sigma} \right] \dot{t} \dot{\phi} + \frac{1}{\Sigma} [(r^2 + a^2)^2 - \Delta a^2] \dot{\phi}^2 \end{aligned} \quad (75)$$

Since the system conserves two fundamental quantities, the energy  $E$  and the angular momentum  $L$ , the equation turns out to be written

$$E = -g_{t\mu} \dot{x}^\mu = \left( \frac{\Delta(r) - a^2}{\Sigma} \right) \dot{t} + 2a \left[ 1 - \frac{\Delta(r) - a^2}{\Sigma} \right] \dot{\phi}, \quad (76)$$

and

$$L = g_{\phi\mu} \dot{x}^\mu = -2a \left[ 1 - \frac{\Delta(r) - a^2}{\Sigma} \right] \dot{t} + \frac{1}{\Sigma} [(r^2 + a^2)^2 - \Delta a^2] \dot{\phi}. \quad (77)$$

To streamline the procedure for solving Eqs. (76) and (77), a more convenient notation is introduced, defined below:

$$E = A\dot{t} + B\dot{\phi}, \quad (78)$$

and

$$L = -B\dot{t} + C\dot{\phi}, \quad (79)$$

where the shorthand notation is defined by  $A \equiv \frac{\Delta(r) - a^2}{\Sigma}$ ,  $B \equiv a \left[ 1 - \frac{\Delta(r) - a^2}{\Sigma} \right]$ , and  $C \equiv \frac{1}{\Sigma} [(r^2 + a^2)^2 - \Delta a^2]$ . It is important to note that

$$CE - BL = (AC + B^2)\dot{t} = \Delta(r)\dot{t} \quad (80)$$

and also

$$AL + BE = (AC + B^2)\dot{\phi} = \Delta(r)\dot{\phi}, \quad (81)$$

in which  $AC + B^2 = \Delta(r)$ . Thereby,

$$\dot{t} = \frac{1}{\Delta(r)} \left[ \frac{1}{\Sigma} [(r^2 + a^2)^2 - \Delta a^2] E - a \left[ 1 - \frac{\Delta(r) - a^2}{\Sigma} \right] L \right], \quad (82)$$

$$\dot{\phi} = \frac{1}{\Delta(r)} \left[ \left( \frac{\Delta(r) - a^2}{\Sigma} \right) L + a \left[ 1 - \frac{\Delta(r) - a^2}{\Sigma} \right] E \right]. \quad (83)$$

The next step involves deriving the expression for the radial component of the four-velocity, rewritten in terms of the parameters  $A$ ,  $B$ , and  $C$  defined earlier:

$$\begin{aligned} g_{\mu\nu}\dot{x}^\mu\dot{x}^\nu &= \mathcal{L} \\ &= -A\dot{t}^2 - 2B\dot{t}\dot{\phi} + C\dot{\phi}^2 + D\dot{r}^2 \\ &= -[A\dot{t} + B\dot{\phi}]\dot{t} + [-B\dot{t} + C\dot{\phi}]\dot{\phi} + \frac{\Sigma}{\Delta(r)}\dot{r}^2 \\ &= -E\dot{t} + L\dot{\phi} + \frac{D}{\Delta(r)}\dot{r}^2, \end{aligned} \quad (84)$$

where  $D \equiv \Sigma$ . With this definition, the radial equation can be expressed as

$$\begin{aligned} \dot{r}^2 &= \frac{\Delta(r)}{D} (E\dot{t} - L\dot{\phi} + \mathcal{L}) \\ &= \frac{1}{D} [CE^2 - 2BLE - AL^2 + \Delta(r)\mathcal{L}]. \end{aligned} \quad (85)$$

It is worth pointing out that

$$CE^2 - 2BLE - AL^2 + \mathcal{L} = (E - \mathcal{V}_-)(E + \mathcal{V}_+), \quad (86)$$

with  $\mathcal{V}_\pm = \frac{\pm\sqrt{ACL^2+B^2L^2-C\mathcal{L}+BL}}{C}$ , which results in the following expression

$$\dot{r}^2 = \frac{1}{D} [(E - \mathcal{V}_-)(E + \mathcal{V}_+)]. \quad (87)$$

Explicitly,  $\mathcal{V}_\pm$  can be expressed as

$$\mathcal{V}_\pm = \frac{\pm 4Mr \sqrt{\frac{64M(L^2r(a^2+r(r-2M)) - \mathcal{L}(a^2(2M+r)+r^3)) + 2\Theta^2(a^2\mathcal{L} + L^2r^2)}{Mr}} + aL(64M^2 - \Theta^2)}{32M(a^2(2M+r) + r^3) - a^2\Theta^2}. \quad (88)$$

Figs. 12 and 13 depict the behavior of the potentials  $\mathcal{V}_\pm$  in the timelike case, where  $\mathcal{L} = -1$ . In Fig. 12, the dependence of  $\mathcal{V}_+$  on the radial coordinate  $r$  is shown. The left panel examines how the potential responds to variations in  $a$  with  $\Theta$  held constant, while the right panel illustrates the influence of different values of  $\Theta$  for a fixed  $a$ . Likewise, Fig. 13 presents the radial profile of  $\mathcal{V}_-$ , using identical parameter choices for both  $a$  and  $\Theta$ , enabling a straightforward comparison between the two potentials. To further clarify the geodesic motion, Fig. 14 provides a detailed visualization of the particle trajectories.

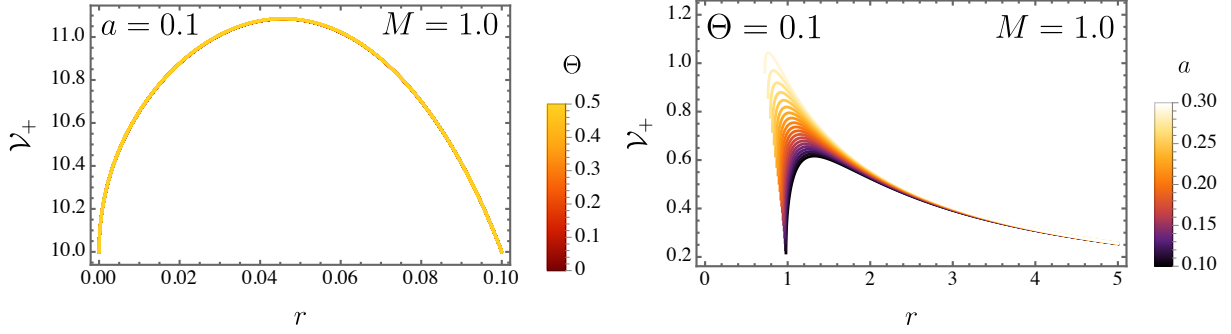


Figure 12: The potential  $\mathcal{V}_+$  is illustrated for various combinations of the rotational parameter  $a$  and the non-commutative parameter  $\Theta$ .

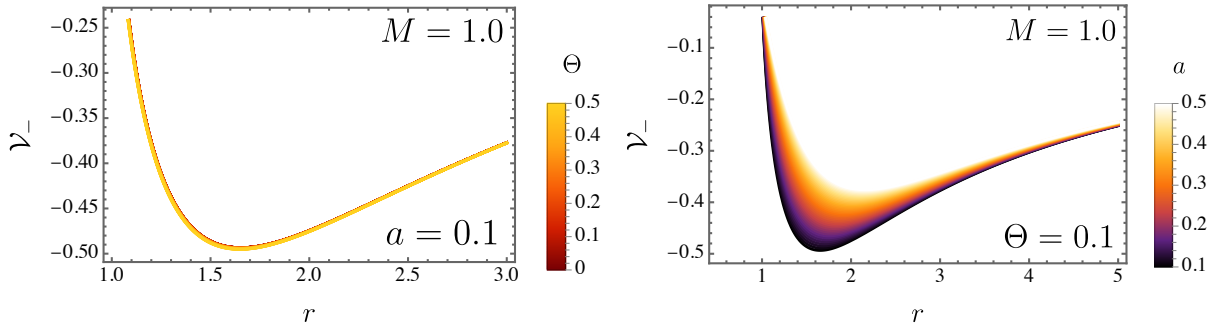


Figure 13: The potential  $\mathcal{V}_-$  is shown for different values of the rotational parameter  $a$  and the non-commutative parameter  $\Theta$ .

### A. The radial acceleration analysis for null geodesics

For null geodesics, the radial equation (87) simplifies to

$$\dot{r}^2 = \frac{1}{D} (E - \mathcal{V}_-) (E + \mathcal{V}_+).$$

Null geodesics are physically admissible only if the condition  $\dot{r}^2 \geq 0$  is satisfied. Evaluating this constraint shows that massless particles can traverse null geodesics when the inequality holds. This requirement is met when the energy constant  $E$  lies beyond the bounds set by the potentials, ensuring the existence of the geodesic path. Consequently, null geodesics occur under the condition below:

$$E < \mathcal{V}_- \quad \text{or} \quad E > \mathcal{V}_+.$$

The region defined by  $\mathcal{V}_- < E < \mathcal{V}_+$  remains forbidden for particle trajectories. To further explore the orbital behavior, examining the radial acceleration is necessary. It is achieved

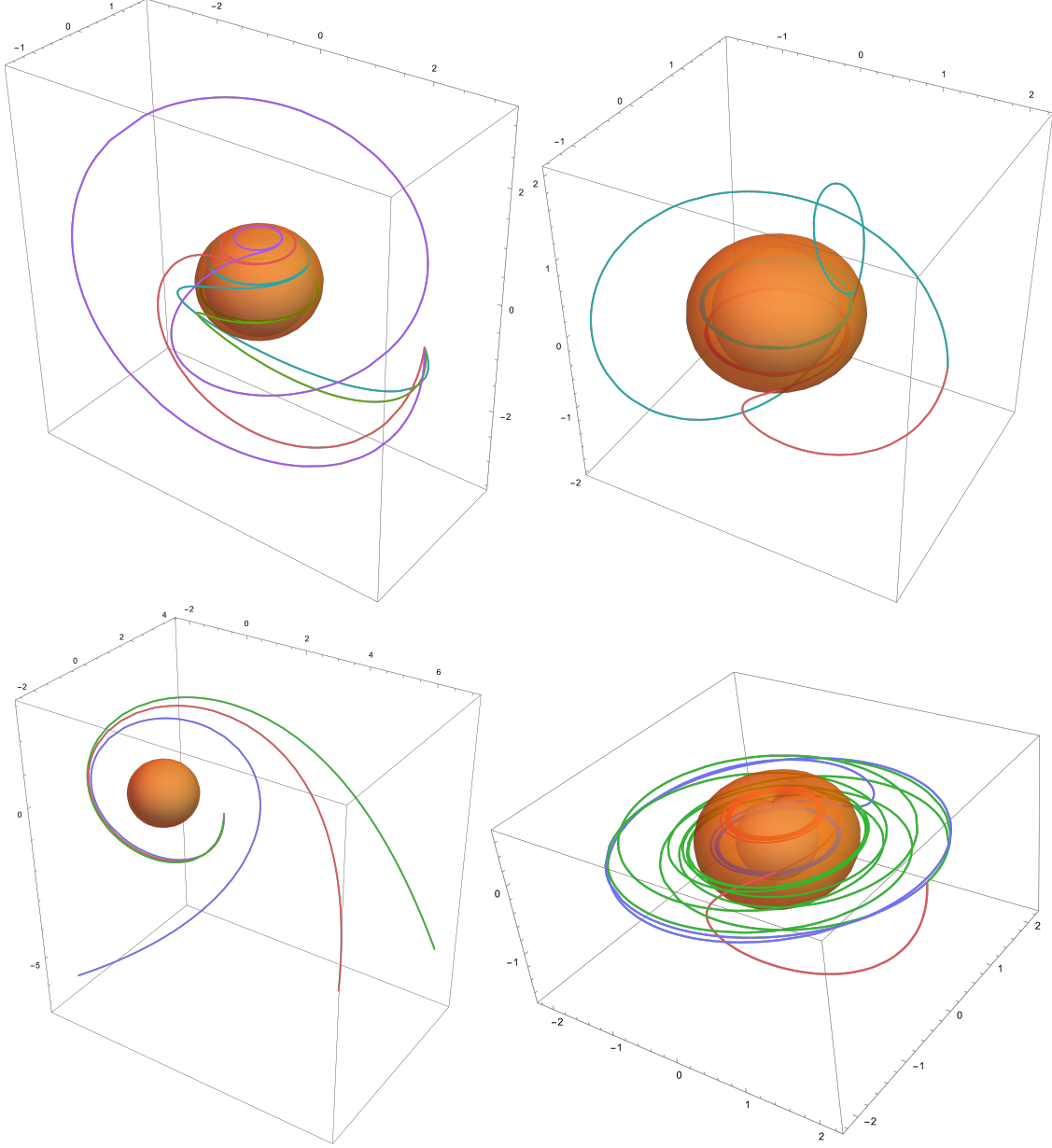


Figure 14: The geodesic trajectories are presented for the configuration with  $\Theta = 0.001$ .

by taking the derivative of Eq. (87) with respect to the affine parameter  $s$ , resulting in

$$2\dot{r}\ddot{r} = \left[ \left( \frac{1}{D} \right)' (E - \mathcal{V}_+)(E - \mathcal{V}_-) - \frac{1}{D} \mathcal{V}'_+(E - \mathcal{V}_-) - \frac{1}{D} \mathcal{V}'_-(E - \mathcal{V}_+) \right] \dot{r}, \quad (89)$$

or, in other words,

$$\ddot{r} = \frac{1}{2} \left( \frac{1}{D} \right)' (E - \mathcal{V}_+)(E - \mathcal{V}_-) - \frac{1}{2D} [\mathcal{V}'_+(E - \mathcal{V}_-) - \mathcal{V}'_-(E - \mathcal{V}_+)]. \quad (90)$$

Here, the prime symbol ( $'$ ) represents differentiation with respect to the radial coordinate  $r$ . The radial acceleration is analyzed at positions where the radial velocity  $\dot{r}$  equals zero,

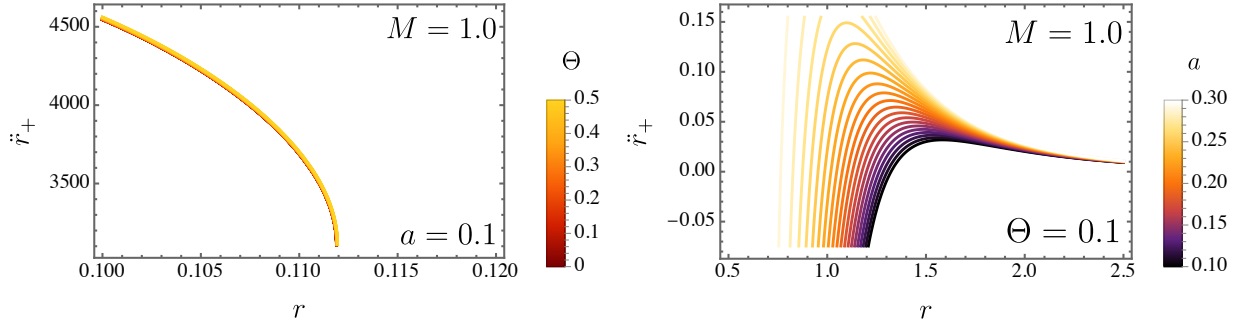


Figure 15: The radial acceleration  $\ddot{r}_+$  is shown as a function of  $r$  for various choices of the parameters  $a$  and  $\Theta$ .

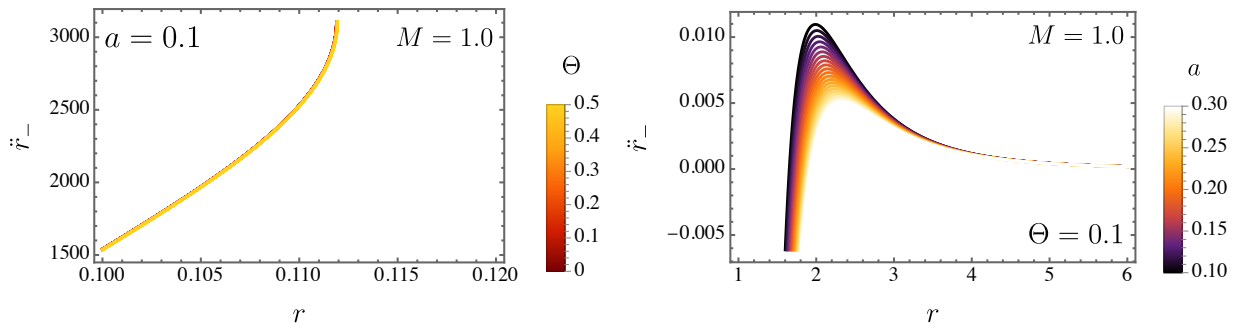


Figure 16: The radial acceleration  $\ddot{r}_-$  is represented as a function of  $r$  for multiple combinations of the parameters  $a$  and  $\Theta$ .

which occurs when the energy parameter  $E$  coincides with one of the potentials, either  $\mathcal{V}_+$  or  $\mathcal{V}_-$

$$\ddot{r}_+ = -\frac{1}{2D}\mathcal{V}'_+(\mathcal{V}_+ - \mathcal{V}_-), \quad \text{if } E = \mathcal{V}_+, \quad (91)$$

and also

$$\ddot{r}_- = -\frac{1}{2D}\mathcal{V}'_-(\mathcal{V}_- - \mathcal{V}_+), \quad \text{if } E = \mathcal{V}_-, \quad (92)$$

where  $r_{\pm}$  correspond to the radial accelerations. To illustrate the behavior of  $\ddot{r}_{\pm}$  more clearly, Figs. 15 and 16 are included for reference.

## VII. SHADOWS

Photon geodesics are entirely governed by the geometry and symmetries of the spacetime. Consequently, examining null geodesics provides valuable information about the characteristics of the modified gravity theory. In this spacetime, the motion of photons is described



by four constants of motion: the vanishing rest mass  $m = 0$ , the energy  $E = -g_{t\phi}\dot{\phi} - g_{tt}\dot{t}$ , and the azimuthal angular momentum  $L_z = g_{\phi\phi}\dot{\phi} + g_{\phi t}\dot{t}$ . Additionally, the Carter constant  $Q$ , arising from a hidden symmetry, allows the equations for null geodesics to be expressed in a first-order form. These equations can be derived using Carter's formalism through the Hamilton–Jacobi equation, as demonstrated as follows

$$\begin{aligned}
\Sigma\dot{t} &= \frac{r^2 + a^2}{\Delta} [E(r^2 + a^2) - aL_z] - a(aE \sin^2 \theta - L_z), \\
\Sigma\dot{\phi} &= \frac{a}{\Delta} [E(r^2 + a^2) - aL_z] - \left( aE - \frac{L_z}{\sin^2 \theta} \right), \\
\Sigma^2\dot{r}^2 &= [(r^2 + a^2) - aL_z]^2 - \Delta(r) [\mathcal{K} + (aE - L_z)^2] \equiv \mathcal{R}(r), \\
\Sigma^2\dot{\theta}^2 &= \mathcal{K} - \left( \frac{L_z^2}{\sin^2 \theta} - a^2 E^2 \right) \cos^2 \theta \equiv \tilde{\Theta}(r).
\end{aligned} \tag{93}$$

Now, let us re-scaled energy parameters  $\xi = L/E$  and  $\eta = K/E^2$ , referred to as critical impact parameters within the expressions for  $R(r)$  and  $\tilde{\Theta}(r)$ . The investigation is limited to the region beyond the event horizon, focusing on spherical photon trajectories — null geodesics confined to specific radii  $r_p$ . These orbits are described by the conditions  $\mathcal{R}'(r_p) = 0$  and  $\mathcal{R}''(r_p) = 0$  for all  $r_p > r_+$  [155]. This formulation allows the determination of critical impact parameters for the non-commutative black hole under study, leading to the following equations:

$$\begin{aligned}
\xi_c &= \frac{(a^2 + r^2)\Delta'(r) - 4r\Delta(r)}{a\Delta'(r)}, \\
\eta_c &= \frac{r^2(8\Delta(r)(2a^2 + r\Delta'(r)) - r^2\Delta'^2(r) - 16\Delta^2(r))}{a^2\Delta'^2(r)}.
\end{aligned} \tag{94}$$

Spherical photon orbits are confined within a three-dimensional region called the photon shell, which defines the bright boundary of the black hole shadow. This region is described by several parameters: the time coordinate  $t$ , ranging from  $-\infty$  to  $\infty$ ; the radial position  $r_p$  within the interval  $r_{p-}$  to  $r_{p+}$ ; the azimuthal angle  $\phi$ , varying between 0 and  $2\pi$ ; and the polar angle  $\theta$ , which spans from  $\theta_-$  to  $\theta_+$ , where  $\theta_{\mp} = \arccos(\mp\sqrt{\tilde{\omega}})$

$$\tilde{\omega} = \frac{a^2 - \eta_c - \xi_c^2 + \sqrt{(a^2 - \eta_c - \xi_c^2)^2 + 4a^2\eta_c}}{2a^2}. \tag{95}$$

To clarify the results further, Fig. 17 displays the three-dimensional representation of  $\theta_+$ ,  $\theta_-$ , and the combined range  $\theta_+ + \theta_-$ .

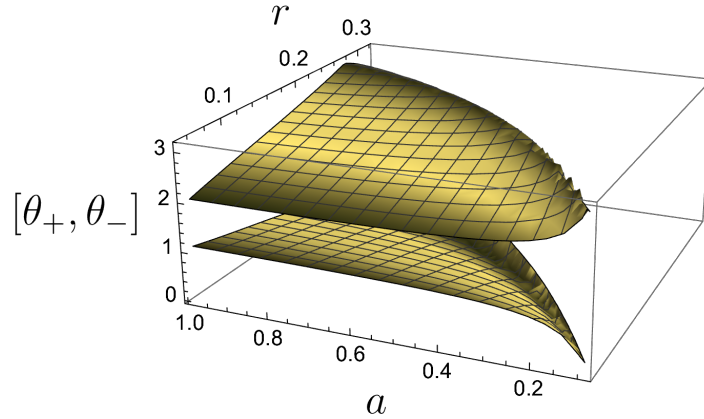


Figure 17: Parameters  $\theta_+$  and  $\theta_-$  are shown for different  $a$  and for a fixed value of  $\Theta = 0.1$ .

The radii  $r_{p\mp}$  correspond to the prograde and retrograde photon orbits, respectively, and are obtained by solving the equation  $\eta_c = 0$  under the constraint  $\xi_c(r_{p\mp}) \geq 0$ . The explicit expression for  $r_p$  is given by

$$r_p = - \frac{(-64M^3 + \Theta^2 M + \sqrt[3]{\tilde{\psi}})^2}{64M^2 \sqrt[3]{\tilde{\psi}}}, \quad (96)$$

in which

$$\begin{aligned} \tilde{\psi} = & 128 \sqrt{a^2 M^8 (\Theta^2 - 64M^2)^2 (4096a^2 M^2 + (\Theta^2 - 64M^2)^2)} \\ & + 8192a^2 (64M^7 - \Theta^2 M^5) + (64M^3 - \Theta^2 M)^3. \end{aligned} \quad (97)$$

The point where photons shift from prograde to retrograde orbits is marked by the intermediate radius  $r_{p0}$ , derived from the condition  $\xi_c = 0$ . At this radius, spherical photon orbits occur with zero angular momentum, and it can be described by

$$r_{p0} = \frac{\frac{18(4096a^2 M^2 + (\Theta^2 - 64M^2)^2)}{\sqrt[3]{\lambda^\dagger}} + 18\sqrt[3]{\lambda^\dagger} + 18(64M^2 - \Theta^2)}{1152M}, \quad (98)$$

where

$$\lambda^\dagger = 64 \sqrt{-a^2 M^2 (4096a^2 M^2 + (\Theta^2 - 64M^2)^2)^2 + 4096a^2 (64M^4 - \Theta^2 M^2) + (64M^2 - \Theta^2)^3}. \quad (99)$$

Spherical photon orbits within the photon shell typically exhibit oscillatory motion along the  $\theta$ -direction, varying between the polar angles  $\theta_\mp$  [216]. In contrast, at the outer and inner limits of the shell, located at  $r = r_{p\mp}$ , the motion becomes restricted to the equatorial plane ( $\theta = \pi/2$ ), where the orbits reduce to planar trajectories [216, 217].

The black hole shadow's shape is influenced by its spin, additional spacetime parameters, and the observer's viewing angle  $\theta_0$  relative to the spin axis. The overall size of the shadow is determined by the black hole's mass  $M$ . For an observer located at  $r_0 \rightarrow \infty$  and viewing from an inclination angle  $\theta_0$ , the shadow manifests as a dark silhouette against a luminous background, described using the following celestial coordinates

$$\{\tilde{\alpha}, \tilde{\beta}\} = \left\{ -\xi_c \csc \theta_0, \pm \sqrt{\eta_c + a^2 \cos^2 \theta_0 - \xi_c^2 \cot^2 \theta_0} \right\}. \quad (100)$$

To better illustrate the results, Fig. 18 shows the evolution of black hole shadows under different configurations of the spin parameter  $a$  and the non-commutative parameter  $\Theta$ . The left panel explores the impact of varying  $a$  while keeping  $\Theta$  fixed. The gray curve corresponds to the shadow of a Schwarzschild black hole, serving as a reference. The colored curves represent progressively increasing values of  $a$ , ranging from 0.1 to 0.99 in steps of 0.1, highlighting how the shadow shape becomes more distorted with higher spin.

In the right panel, the focus shifts to the effect of varying the non-commutative parameter  $\Theta$  while holding the spin parameter constant at  $a = 0.1$ . The values of  $\Theta$  span from 0.1 to 1.0, increasing from left to right. Although the shadows may seem almost circular at first glance, they are in fact slightly elliptical. This subtle deviation is particularly noticeable in the red curve, where the difference from the gray reference circle becomes clearer, confirming that the colored curves represent ellipses rather than perfect circles.

## VIII. GRAVITATIONAL LENSING IN THE STRONG DEFLECTION REGIME

Let us start with the Lagrangian written below

$$\mathcal{L} = \frac{1}{2} g_{\mu\nu}^{\Theta} u^{\mu} u^{\nu}. \quad (101)$$

A particle's motion can be described using the 4-velocity  $u^{\mu} = d^{\mu}/d\lambda$ , where  $\lambda$  serves as an affine parameter. Due to the stationarity and axisymmetry of our metric displayed in Eq. (38), its invariance under translations in  $t$  and  $\phi$  results in the presence of two Killing vectors,  $\xi_{(t)}^{\mu}$  and  $\xi_{(\phi)}^{\mu}$  as

$$\xi_{(t)}^{\mu} = \delta_t^{\mu}, \quad \xi_{(\phi)}^{\mu} = \delta_{\phi}^{\mu}. \quad (102)$$

The conserved quantities associated with a geodesic can be determined using the Killing vectors in conjunction with the 4-velocity of light rays. These quantities are expressed as

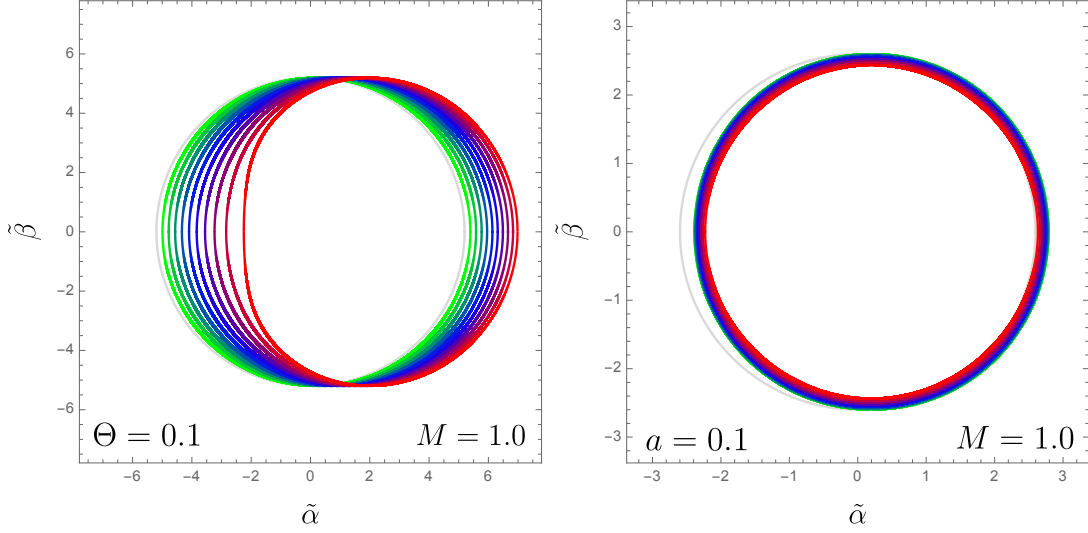


Figure 18: The shadows are presented for various configurations of the non–commutative parameter  $\Theta$  and the spin parameter  $a$ .

$\varepsilon = -\xi_{(t)}^\mu u_\mu$ ,  $\ell = \xi_{(\phi)}^\mu u_\mu$ , where  $\varepsilon$  represents the energy of the light ray, and  $\ell$  corresponds to its azimuthal angular momentum as measured at spatial infinity. Since light rays follow null geodesics, their 4–velocity satisfies the constraint  $u^\mu u_\mu = 0$ . To distinguish whether the motion aligns with or opposes the frame–dragging effect, the impact parameter is introduced as follows:

$$b_s = s \left| \frac{\ell}{\varepsilon} \right| \equiv s b. \quad (103)$$

To characterize the direction of a light ray’s motion relative to the frame-dragging effect, the parameter  $s = \text{Sign}(\ell/\varepsilon)$  is introduced, where  $b$  represents its absolute value. When  $s = +1$  and  $b_s > 0$ , the trajectory follows a direct orbit, whereas  $s = -1$  with  $b_s < 0$  corresponds to a retrograde path, following a specific sign convention. For simplicity, attention is restricted to light rays propagating within the equatorial plane of the black hole, imposing the conditions  $\theta = \pi/2$  and  $\dot{\theta} = 0$ . Under this assumption, the radial equation of motion can be rewritten in the form presented in [218, 219]

$$\frac{1}{b^2} = \frac{\dot{r}^2}{\ell^2} + \tilde{\mathcal{V}}^\dagger(r), \quad (104)$$

and based on this formulation, the function  $\tilde{\mathcal{V}}^\dagger$  is introduced as

$$\tilde{\mathcal{V}}^\dagger(r) = \frac{1}{r^2} \left[ 1 - \frac{a^2}{b^2} - \frac{2M\Theta}{r} \left( 1 - \frac{a}{b_s} \right)^2 \right]. \quad (105)$$

The equation governing the radial motion resembles that of a particle moving under an effective potential  $\tilde{\mathcal{V}}^\dagger(r)$ , where the term  $\dot{r}^2/\ell^2$  plays the role of kinetic energy, and the total energy remains fixed at  $1/b^2$ . Consider a scenario in which a light ray originates from a distant region, moves toward the black hole, and then returns to the asymptotic region before reaching an observer. Such trajectories exhibit a turning point, corresponding to the closest approach distance  $r_0$  to the black hole. This critical distance is dictated by the impact parameter  $b$ , which is determined through the condition:

$$\left. \frac{\dot{r}^2}{\ell^2} \right|_{r=r_0} = \frac{1}{b^2} - \tilde{\mathcal{V}}^\dagger(r_0) = 0. \quad (106)$$

Using Eq. (106), as also demonstrated in [218–220], the impact parameter  $b$  can be expressed in terms of the closest approach distance  $r_0$ . This relation serves as a key input for deriving analytical expressions for the deflection angle within the strong deflection limit (SDL), given by:

$$b(r_0) = \frac{2sM_\Theta a - r_0 \sqrt{a^2 - 2r_0 M_\Theta + r_0^2}}{2M_\Theta - r_0}. \quad (107)$$

The nature of light ray trajectories is dictated by the relationship between  $1/b^2$  and the peak value of the effective potential  $\tilde{\mathcal{V}}^\dagger(r)$ . The innermost paths followed by light rays play a fundamental role in shaping the observed silhouette of the black hole. The smallest possible radius, denoted as  $r_{sc}$ , corresponds to the turning point  $r_0$  being precisely at the maximum of  $\tilde{\mathcal{V}}^\dagger(r)$ . At this critical location, the impact parameter takes the value  $b_{sc}$ , satisfying the condition:

$$\left. \frac{d\tilde{\mathcal{V}}^\dagger(r)}{dr} \right|_{r=r_{sc}} = 0. \quad (108)$$

The radius at which light follows a circular trajectory, defining the photon sphere, is determined by the condition at which the turning point coincides with the maximum of the effective potential. This characteristic radius is given by (see [218–220])

$$r_{sc} = 2M_\Theta \left\{ 1 + \cos \left[ \frac{2}{3} \cos^{-1} \left( \frac{-sa}{M_\Theta} \right) \right] \right\} \quad (109)$$

where the impact parameter reads

$$b_{sc} = -a + s6M_\Theta \cos \left[ \frac{1}{3} \cos^{-1} \left( \frac{-sa}{M_\Theta} \right) \right]. \quad (110)$$

For our rotating non-commutative solution, the black hole's spin enhances the repulsive effects on light rays in direct orbits more than in retrograde ones due to the  $1/r^3$  term in

the effective potential. This repulsion prevents direct orbit trajectories from collapsing into the event horizon, shifting the innermost circular paths inward. Consequently, the critical impact parameter in direct orbits,  $b_{+c}$ , is smaller than  $b_{-c}$  for retrograde ones. As the spin parameter  $a$  increases, the critical impact parameter  $b_{+c}$  decreases, while  $|b_{-c}|$  grows instead [218–220]. Additionally, the black hole’s rotation reduces the deflection angle for direct orbits compared to retrograde ones when both share the same impact parameter  $b$  [218–220].

Next, let us introduce a new variable

$$z \equiv 1 - \frac{r_0}{r}. \quad (111)$$

The geodesic equations governing  $r$  and  $\phi$ , as derived in [218, 219], can be reformulated using the variable  $z$ , following the approach in [221]

$$\frac{dz}{d\phi} = \frac{1}{r_0} \frac{1 - \frac{2M_\Theta}{r_0}(1-z) + \frac{a^2}{r_0^2}(1-z)^2}{1 - \frac{2M_\Theta}{r_0}(1-z)(1 - \frac{a}{b_s})} \sqrt{B(z, r_0)}. \quad (112)$$

Here, the function  $B(z, r_0)$  takes the form of a trinomial expression in terms of  $z$ .

$$B(z, r_0) = c_1(r_0)z + c_2(r_0)z^2 + c_3(r_0)z^3, \quad (113)$$

where

$$\begin{aligned} c_1(r_0) &= -6M_\Theta r_0 \left(1 - \frac{a}{b_s}\right)^2 + 2r_0^2 \left(1 - \frac{a^2}{b^2}\right), \\ c_2(r_0) &= 6M_\Theta r_0 \left(1 - \frac{a}{b_s}\right)^2 - r_0^2 \left(1 - \frac{a^2}{b^2}\right), \\ c_3(r_0) &= -2M_\Theta r_0 \left(1 - \frac{a}{b_s}\right)^2. \end{aligned} \quad (114)$$

After that, we consider

$$\frac{1 - \frac{2M_\Theta}{r_0}\left(1 - \frac{a}{b_s}\right) + \frac{2M_\Theta}{r_0}\left(1 - \frac{a}{b_s}\right)z}{1 - \frac{2M_\Theta}{r_0} + \frac{a^2}{r_0^2} + \left(\frac{2M_\Theta}{r_0} - \frac{2a^2}{r_0^2}\right)z + \frac{a^2}{r_0^2}z^2} = \frac{r_0^2}{a^2} \left( \frac{C_-}{z - z_-} + \frac{C_+}{z - z_+} \right). \quad (115)$$

Notice that the roots are represented by  $z_-$ ,  $z_+$ , and the coefficients  $C_-$ ,  $C_+$  are [218]

$$\begin{aligned} z_- &= 1 - \frac{r_0 r_-}{a^2}, \\ z_+ &= 1 - \frac{r_0 r_+}{a^2}, \end{aligned} \quad (116)$$

$$\begin{aligned}
C_- &= \frac{a^2 - 2M_\Theta r_- (1 - \frac{a}{b_s})}{2r_0 \sqrt{M_\Theta^2 - a^2}}, \\
C_+ &= \frac{-a^2 + 2M_\Theta r_+ (1 - \frac{a}{b_s})}{2r_0 \sqrt{M_\Theta^2 - a^2}}
\end{aligned} \tag{117}$$

with  $r_+$  and  $r_-$  represent the outer and inner horizons of our black hole solution, as outlined in Sec. IV. Notably, for any value of the spin parameter  $a$ , the roots satisfy  $z_-, z_+ \leq 0$ . Using Eq. (112), the deflection angle can then be expressed as a function of the closest approach distance  $r_0$ , yielding:

$$\hat{\alpha}(r_0) = I(r_0) - \pi, \quad I(r_0) = \int_0^1 f(z, r_0) dz, \tag{118}$$

so that the integrand turns out to be

$$f(z, r_0) = \frac{r_0^2}{a^2} \left( \frac{C_-}{z - z_-} + \frac{C_+}{z - z_+} \right) \frac{2r_0}{\sqrt{c_1(r_0)z + c_2(r_0)z^2 + c_3(r_0)z^3}}. \tag{119}$$

In SDL under consideration, as the closest approach distance approaches its critical value, i.e.,  $r_0 \rightarrow r_{sc}$ , the coefficient  $c_1(r_0)$  in (114), derived from (108), vanishes. Consequently, for small  $z$ , the integrand  $f(z, r_0)$  behaves as  $\frac{1}{z}$ , leading to a logarithmic divergence in the deflection angle as  $r_0 \rightarrow r_{sc}$ . To handle this behavior, we introduce a new function,  $f_D(z, r_0)$

$$f_D(z, r_0) = \frac{r_0^2}{a^2} \left( \frac{C_-}{z - z_-} + \frac{C_+}{z - z_+} \right) \frac{2r_0}{\sqrt{c_1(r_0)z + c_2(r_0)z^2}}. \tag{120}$$

Notice that this function  $f_D(z, r_0)$  isolates the divergent contribution, allowing the remaining part to be expressed as  $f_R(z, r_0) = f(z, r_0) - f_D(z, r_0)$ . Since  $f_R(z, r_0)$  does not exhibit any singularity, its integral remains finite.

The divergence arises from the integral of the function  $f_D(z, r_0)$ , which influences both the coefficient  $\bar{a}$  in the logarithmic term and  $\bar{b}$  in the regular part, leading to

$$\begin{aligned}
I_D(r_0) &= \int_0^1 f_D(z, r_0) dz \\
&= \frac{2r_0^3}{a^2} \frac{C_-}{\sqrt{c_1(r_0)z_- + c_2(r_0)z_-^2}} \ln \left( \frac{\sqrt{c_1(r_0)z_- + c_2(r_0)z_-} + \sqrt{c_1(r_0) + c_2(r_0)z_-}}{\sqrt{c_1(r_0)z_- + c_2(r_0)z_-} - \sqrt{c_1(r_0) + c_2(r_0)z_-}} \right) \\
&\quad + \frac{2r_0^3}{a^2} \frac{C_+}{\sqrt{c_1(r_0)z_+ + c_2(r_0)z_+^2}} \ln \left( \frac{\sqrt{c_1(r_0)z_+ + c_2(r_0)z_+} + \sqrt{c_1(r_0) + c_2(r_0)z_+}}{\sqrt{c_1(r_0)z_+ + c_2(r_0)z_+} - \sqrt{c_1(r_0) + c_2(r_0)z_+}} \right).
\end{aligned} \tag{121}$$

In SDL, the coefficient  $c_1(r_0)$  from (114) and the impact parameter  $b(r_0)$  can be expanded as power series in terms of the small deviation  $r_0 - r_{sc}$  as follows

$$c_1(r_0) = c'_{1sc}(r_0 - r_{sc}) + O(r_0 - r_{sc})^2, \tag{122}$$

$$b(r_0) = b_{sc} + \frac{b''_{sc}}{2!}(r_0 - r_{sc})^2 + O(r_0 - r_{sc})^3. \quad (123)$$

Here, it is important to mention that  $c_1(r_{sc}) \equiv c_{1sc} = 0$ , while  $b(r_{sc}) \equiv b_{sc}$  corresponds to the critical impact parameter given by (110). The subscript  $sc$  indicates evaluation at  $r = r_{sc}$ , and the prime denotes differentiation with respect to  $r_0$ . Substituting  $c_{1sc} = 0$  into (114), we obtain

$$c_{3sc} = -\frac{2}{3}c_{2sc}. \quad (124)$$

If we combine (122) with (123), the coefficient  $c_1(r_0)$  may be rewritten in terms of the small deviation  $b - b_{sc}$  as:

$$\lim_{r_0 \rightarrow r_{sc}} c_1(r_0) = \lim_{b \rightarrow b_{sc}} c'_{1sc} \sqrt{\frac{2b_{sc}}{b''_{sc}}} \left( \frac{b}{b_{sc}} - 1 \right)^{1/2}. \quad (125)$$

In this manner, substituting (125) into (121) transforms  $I_D$  into [218]

$$\begin{aligned} I_D(b) \simeq & - \left( \frac{r_{sc}^3}{a^2} \frac{C_{-sc}}{\sqrt{c_{2sc} z_{-sc}^2}} + \frac{r_{sc}^3}{a^2} \frac{C_{+sc}}{\sqrt{c_{2sc} z_{+sc}^2}} \right) \ln \left( \frac{b}{b_{sc}} - 1 \right) \\ & + \frac{r_{sc}^3}{a^2} \frac{C_{-sc}}{\sqrt{c_{2sc} z_{-sc}^2}} \ln \left( \frac{16 c_{2sc}^2 z_{-sc}^2 b''_{sc}}{c_{1sc}^2 2b_{sc} (z_{-sc} - 1)^2} \right) + \frac{r_{sc}^3}{a^2} \frac{C_{+sc}}{\sqrt{c_{2sc} z_{+sc}^2}} \ln \left( \frac{16 c_{2sc}^2 z_{+sc}^2 b''_{sc}}{c_{1sc}^2 2b_{sc} (z_{+sc} - 1)^2} \right). \end{aligned} \quad (126)$$

Finally, the coefficient  $\bar{a}$  and the portion of  $I_D(b)$  contributing to  $\bar{b}$ , referred to as  $b_D$ , are expressed as:

$$\bar{a} = \frac{r_{sc}^3}{\sqrt{c_{2sc}}} \left[ \frac{C_{-sc}}{r_{sc} r_- - a^2} + \frac{C_{+sc}}{r_{sc} r_+ - a^2} \right] \quad (127)$$

as well as

$$b_D = \bar{a} \ln \left[ \frac{8c_{2sc}^2 b''_{sc}}{c_{1sc}^2 b_{sc}} \right] + \frac{2r_{sc}^3}{\sqrt{c_{2sc}}} \left[ \frac{C_{-sc}}{r_{sc} r_- - a^2} \ln \left( 1 - \frac{a^2}{r_{sc} r_-} \right) + \frac{C_{+sc}}{r_{sc} r_+ - a^2} \ln \left( 1 - \frac{a^2}{r_{sc} r_+} \right) \right]. \quad (128)$$

By expressing  $z_{\pm}$  in terms of  $r_{\pm}$  using (116), the integration of  $f_R(z, r_{sc})$  in SDL yields the leading-order contribution to the coefficient  $\bar{b}$ . This contribution, labeled as  $b_R$ , is given



by [218]

$$\begin{aligned}
b_R &= I_R(r_{sc}) = \int_0^1 f_R(z, r_{sc}) dz \\
&= \frac{2r_0^3}{a^2} \frac{C_-}{\sqrt{c_2} z_-} \ln \left( \frac{z_-}{z_- - 1} \frac{\sqrt{c_2 + c_3} + \sqrt{c_2}}{\sqrt{c_2 + c_3} - \sqrt{c_2}} \frac{c_3}{4c_2} \right) \\
&\quad + \frac{2r_0^3}{a^2} \frac{C_-}{\sqrt{c_2 + c_3} z_-} \ln \left( \frac{\sqrt{c_2 + c_3} z_- - \sqrt{c_2 + c_3}}{\sqrt{c_2 + c_3} z_- + \sqrt{c_2 + c_3}} \frac{\sqrt{c_2 + c_3} z_- + \sqrt{c_2}}{\sqrt{c_2 + c_3} z_- - \sqrt{c_2}} \right) \\
&\quad + \frac{2r_0^3}{a^2} \frac{C_+}{\sqrt{c_2} z_+} \ln \left( \frac{z_+}{z_+ - 1} \frac{\sqrt{c_2 + c_3} + \sqrt{c_2}}{\sqrt{c_2 + c_3} - \sqrt{c_2}} \frac{c_3}{4c_2} \right) \\
&\quad + \frac{2r_0^3}{a^2} \frac{C_+}{\sqrt{c_2 + c_3} z_+} \ln \left( \frac{\sqrt{c_2 + c_3} z_+ - \sqrt{c_2 + c_3}}{\sqrt{c_2 + c_3} z_+ + \sqrt{c_2 + c_3}} \frac{\sqrt{c_2 + c_3} z_+ + \sqrt{c_2}}{\sqrt{c_2 + c_3} z_+ - \sqrt{c_2}} \right) \Big|_{r_0=r_{sc}}.
\end{aligned} \tag{129}$$

Therefore, the coefficient  $\bar{b}$  is determined by the sum of  $b_D$  and  $b_R$ , which reads

$$\bar{b} = -\pi + b_D + b_R, \tag{130}$$

where by utilizing (128) and (129), along with the substitutions from (124) and (116), we express  $c_{3sc}$  in terms of  $c_{2sc}$  as  $c_{2sc} = -\frac{2}{3}c_{3sc}$  and replace  $z_{\pm}$  with  $r_{\pm}$ . After performing the necessary algebraic manipulations, we get [218]

$$\begin{aligned}
\bar{b} &= -\pi + \bar{a} \ln \left( \frac{36}{7 + 4\sqrt{3}} \frac{8c_{2sc}^2 b_{sc}''}{c_{1sc}^2 b_{sc}} \right) \\
&\quad + \frac{r_{sc}^3}{\sqrt{c_{2sc}}} \frac{2aC_{-sc}}{a^2 - r_{sc}r_-} \frac{\sqrt{3}}{\sqrt{a^2 + 2r_{sc}r_-}} \ln \left( \frac{\sqrt{a^2 + 2r_{sc}r_-} - a}{\sqrt{a^2 + 2r_{sc}r_-} + a} \frac{\sqrt{a^2 + 2r_{sc}r_-} + \sqrt{3}a}{\sqrt{a^2 + 2r_{sc}r_-} - \sqrt{3}a} \right) \\
&\quad + \frac{r_{sc}^3}{\sqrt{c_{2sc}}} \frac{2aC_{+sc}}{a^2 - r_{sc}r_+} \frac{\sqrt{3}}{\sqrt{a^2 + 2r_{sc}r_+}} \ln \left( \frac{\sqrt{a^2 + 2r_{sc}r_+} - a}{\sqrt{a^2 + 2r_{sc}r_+} + a} \frac{\sqrt{a^2 + 2r_{sc}r_+} + \sqrt{3}a}{\sqrt{a^2 + 2r_{sc}r_+} - \sqrt{3}a} \right).
\end{aligned} \tag{131}$$

By employing the expressions for  $r_{sc}$  in (109),  $b_{sc}$  in (110), and  $b(r_0)$  in (107), along with the definitions of  $C_{\pm}$  and  $c_2$  from (117) and (114), the coefficients  $\bar{a}$  and  $\bar{b}$  from (127) and (131) can be determined. For the parameter range considered,  $\bar{a}$  remains positive, while  $\bar{b}$  is negative. Additionally, both  $\bar{a}$  and  $|\bar{b}|$  increase with  $a$  in direct orbits and decrease in retrograde ones. Consequently, the deflection angle  $\hat{\alpha}$  reduces for direct trajectories and increases for retrograde ones as the black hole's spin grows, given a fixed impact parameter.

The expressions for  $\bar{a}$  and  $\bar{b}$  corresponding to the Schwarzschild black hole, as presented in [218, 221, 222], can be recovered by taking the limit  $a \rightarrow 0$ . In this case, the parameters transform as follows:  $r_+ \rightarrow 2M_{\Theta}$ ,  $r_- \rightarrow a^2/2M_{\Theta}$ ,  $C_{+sc} \rightarrow 2M_{\Theta}/r_{sc}$ ,  $C_{-sc} \rightarrow a^3/(2b_{sc}M_{\Theta}r_{sc})$ , and  $c_{2sc} \rightarrow r_{sc}^2$  with  $c_{1sc} = 0$ . It can be verified that in this limit,  $\bar{a} = 1$  in (127), and  $\bar{b}$  in

(131) simplifies to an expression proportional to  $\bar{a}$ , as outlined below

$$\begin{aligned}\bar{b} &= -\pi + \bar{a} \ln \left( 36(7 - 4\sqrt{3}) \frac{8c_{2sc}^2 b_{sc}''}{c_{1sc}'^2 b_{sc}} \right) \\ &= -\pi + \ln \left( 216(7 - 4\sqrt{3}) \right).\end{aligned}\tag{132}$$

It is worth mentioning that, in the second equality, additional substitutions have been applied based on the Schwarzschild black hole case, where  $r_{sc} = 3M_\Theta$ . These include  $b_{sc} \rightarrow 3\sqrt{3}M_\Theta$ ,  $b_{sc}'' \rightarrow \sqrt{3}/M_\Theta$ ,  $c_{1sc}' \rightarrow 6M_\Theta$ , and  $c_{2sc} \rightarrow 9M_\Theta^2$ .

## IX. CONCLUSION

In this work, we began by analyzing a spherically symmetric black hole within the context of non-commutative gauge theory. Using a modified Newman–Janis algorithm, we obtained a new rotating black hole solution. The physical properties of this solution were then investigated, with particular focus on the event horizon structure, which revealed the presence of both an inner horizon  $r_-$  and an outer horizon  $r_+$ . It was observed that as the non-commutative parameter  $\Theta$  and the rotation parameter  $a$  increased, the horizon radii diminished.

The analysis also extended to the ergosphere, where both an inner boundary  $r_{e-}$  and an outer boundary  $r_{e+}$  were identified. Similar to the event horizons, the ergospheres contracted as  $\Theta$  and  $a$  increased. Additionally, the angular velocity was examined, revealing a reduction in magnitude with increasing  $\Theta$ , while growing with  $a$  up to approximately  $r \approx 2$ . The influence of non-commutativity on the angular velocity was then compared to the standard Kerr case ( $\Theta = 0$ ).

To conduct a comprehensive thermodynamic analysis, we determined the surface gravity, which was crucial for evaluating key thermodynamic quantities such as the Hawking temperature, entropy, and heat capacity. Both the Hawking temperature and entropy exhibited a decreasing trend with increasing  $a$  and, for small values of  $M$ , also with increasing  $\Theta$ . The remnant mass was examined by imposing the extremal black hole condition  $T \rightarrow 0$ , yielding  $M_\pm(a, \Theta) = \frac{1}{8} (\sqrt{16a^2 + \Theta^2} \pm 4a)$ . Meanwhile, the heat capacity displayed an overall split as  $a$  and  $\Theta$  grew, taking on both positive and negative values. All findings were compared to the standard Kerr case ( $\Theta = 0$ ).

Quantum radiation was also examined for our axisymmetric non-commutative black hole

solution. Both bosonic and fermionic particle modes were considered, leading to the corresponding particle creation densities  $n_b(\omega, \Theta, a, M)$  and  $n_f(\omega, \Theta, a, M)$ , respectively. In both cases, the parameters  $\Theta$  and  $a$  contributed to an overall increase in particle creation densities.

The geodesic motion was also investigated, with numerical simulations in 3D provided for better visualization. Particular attention was given to null geodesics and their associated radial accelerations. Additionally, the photon sphere and black hole shadows were analyzed in detail using analytical methods.

Finally, our investigation focused on gravitational lensing in the strong deflection limit. As a potential extension, applying these analyses to Lorentz-violating scenarios, such as bumblebee [223] and Kalb–Ramond [224] gravities, appears to be a promising direction for further research. These and other related aspects are currently under development.

## ACKNOWLEDGMENTS

A. A. Araújo Filho is supported by Conselho Nacional de Desenvolvimento Científico e Tecnológico (CNPq) and Fundação de Apoio à Pesquisa do Estado da Paraíba (FAPESQ), project No. 150891/2023-7. Furthermore, the authors thank M. Ostroff for the valuable discussions and for providing the code used to compute the geodesic segment. A. Ö. would like to acknowledge the contribution of the COST Action CA21106 - COSMIC WISPerS in the Dark Universe: Theory, astrophysics and experiments (CosmicWISPerS), the COST Action CA22113 - Fundamental challenges in theoretical physics (THEORY-CHALLENGES) and CA23130 - Bridging high and low energies in search of quantum gravity (BridgeQG). We also thank TUBITAK and SCOAP3 for their support.

- 
- [1] A. F. Ferrari, H. O. Girotti, M. Gomes, A. Y. Petrov, A. Ribeiro, and A. Da Silva, “On the finiteness of noncommutative supersymmetric qed3 in the covariant superfield formulation,” *Physics Letters B*, vol. 577, no. 1-2, pp. 83–92, 2003.
- [2] R. J. Szabo, “Quantum field theory on noncommutative spaces,” *Physics Reports*, vol. 378, no. 4, pp. 207–299, 2003.

- [3] A. F. Ferrari, H. O. Girotti, M. Gomes, A. Y. Petrov, A. Ribeiro, V. O. Rivelles, and A. Da Silva, “Superfield covariant analysis of the divergence structure of noncommutative supersymmetric qed 4,” *Physical Review D*, vol. 69, no. 2, p. 025008, 2004.
- [4] N. Seiberg and E. Witten, “String theory and noncommutative geometry,” *Journal of High Energy Physics*, vol. 1999, no. 09, p. 032, 1999.
- [5] R. J. Szabo, “Symmetry, gravity and noncommutativity,” *Classical and Quantum Gravity*, vol. 23, no. 22, p. R199, 2006.
- [6] A. F. Ferrari, H. O. Girotti, M. Gomes, A. Y. Petrov, A. Ribeiro, V. O. Rivelles, and A. da Silva, “Towards a consistent noncommutative supersymmetric yang-mills theory: Superfield covariant analysis,” *Physical Review D*, vol. 70, no. 8, p. 085012, 2004.
- [7] A. H. Chamseddine, “Deforming einstein’s gravity,” *Physics Letters B*, vol. 504, no. 1-2, pp. 33–37, 2001.
- [8] M. Sharif and W. Javed, “Thermodynamics of a bardeen black hole in noncommutative space,” *Canadian Journal of Physics*, vol. 89, no. 10, pp. 1027–1033, 2011.
- [9] R. Banerjee, B. R. Majhi, and S. Samanta, “Noncommutative black hole thermodynamics,” *Physical Review D*, vol. 77, no. 12, p. 124035, 2008.
- [10] A. A. Araújo Filho, J. R. Nascimento, A. Y. Petrov, P. J. Porfírio, and A. Övgün, “Properties of an axisymmetric Lorentzian non-commutative black hole,” *Phys. Dark Univ.*, vol. 47, p. 101796, 2025.
- [11] K. Nozari and B. Fazlpour, “Thermodynamics of noncommutative schwarzschild black hole,” *Modern Physics Letters A*, vol. 22, no. 38, pp. 2917–2930, 2007.
- [12] A. A. Araújo Filho, S. Zare, P. J. Porfírio, J. Kříž, and H. Hassanabadi, “Thermodynamics and evaporation of a modified schwarzschild black hole in a non-commutative gauge theory,” *Physics Letters B*, vol. 838, p. 137744, 2023.
- [13] K. Nozari and B. Fazlpour, “Reissner-nordstr\”{o} m black hole thermodynamics in non-commutative spaces,” *arXiv preprint gr-qc/0608077*, 2006.
- [14] Y. S. Myung, Y.-W. Kim, and Y.-J. Park, “Thermodynamics and evaporation of the non-commutative black hole,” *Journal of High Energy Physics*, vol. 2007, no. 02, p. 012, 2007.
- [15] J. Lopez-Dominguez, O. Obregon, M. Sabido, and C. Ramirez, “Towards noncommutative quantum black holes,” *Physical Review D*, vol. 74, no. 8, p. 084024, 2006.

- [16] P. Nicolini, A. Smailagic, and E. Spallucci, “Noncommutative geometry inspired schwarzschild black hole,” *Physics Letters B*, vol. 632, no. 4, pp. 547–551, 2006.
- [17] S. G. Ghosh, “Noncommutative geometry inspired einstein–gauss–bonnet black holes,” *Classical and Quantum Gravity*, vol. 35, no. 8, p. 085008, 2018.
- [18] P. Nicolini, “Noncommutative black holes, the final appeal to quantum gravity: a review,” *International Journal of Modern Physics A*, vol. 24, no. 07, pp. 1229–1308, 2009.
- [19] K. Nozari and S. H. Mehdipour, “Hawking radiation as quantum tunneling from a non-commutative schwarzschild black hole,” *Classical and Quantum Gravity*, vol. 25, no. 17, p. 175015, 2008.
- [20] H. Lekbich, N. Parbin, D. J. Gogoi, A. E. Boukili, and M. Sedra, “The optical features of noncommutative charged 4d-ads-einstein–gauss–bonnet black hole: shadow and deflection angle,” *The European Physical Journal C*, vol. 84, no. 4, p. 350, 2024.
- [21] S.-W. Wei, P. Cheng, Y. Zhong, and X.-N. Zhou, “Shadow of noncommutative geometry inspired black hole,” *Journal of Cosmology and Astroparticle Physics*, vol. 2015, no. 08, p. 004, 2015.
- [22] M. Sharif and S. Iftikhar, “Shadow of a charged rotating non-commutative black hole,” *The European Physical Journal C*, vol. 76, pp. 1–9, 2016.
- [23] A. Övgün, I. Sakalli, J. Saavedra, and C. Leiva, “Shadow cast of noncommutative black holes in rastall gravity,” *Modern Physics Letters A*, vol. 35, no. 20, p. 2050163, 2020.
- [24] C. Ding, S. Kang, C.-Y. Chen, S. Chen, and J. Jing, “Strong gravitational lensing in a noncommutative black-hole spacetime,” *Physical Review D—Particles, Fields, Gravitation, and Cosmology*, vol. 83, no. 8, p. 084005, 2011.
- [25] R. Saleem and M. I. Aslam, “Observable features of charged kiselev black hole with non-commutative geometry under various accretion flow,” *The European Physical Journal C*, vol. 83, no. 3, pp. 1–14, 2023.
- [26] C. Ding and J. Jing, “Probing spacetime noncommutative constant via charged astrophysical black hole lensing,” *Journal of High Energy Physics*, vol. 2011, no. 10, pp. 1–19, 2011.
- [27] N. Heidari, H. Hassanabadi, A. A. P. Araújo Filho, and J. Kriz, “Exploring non-commutativity as a perturbation in the schwarzschild black hole: quasinormal modes, scattering, and shadows,” *The European Physical Journal C*, vol. 84, p. 566, 2024.

- [28] K. Yakut and P. P. Eggleton, “Evolution of close binary systems,” *The Astrophysical Journal*, vol. 629, no. 2, p. 1055, 2005.
- [29] F. Pretorius, “Evolution of binary black-hole spacetimes,” *Physical review letters*, vol. 95, no. 12, p. 121101, 2005.
- [30] H. Kjeldsen and T. R. Bedding, “Amplitudes of stellar oscillations: the implications for asteroseismology,” *arXiv preprint astro-ph/9403015*, 1994.
- [31] W. Dziembowski and P. R. Goode, “Effects of differential rotation on stellar oscillations—a second-order theory,” *The Astrophysical Journal*, vol. 394, pp. 670–687, 1992.
- [32] W. Unno, Y. Osaki, H. Ando, and H. Shibahashi, “Nonradial oscillations of stars,” *Tokyo: University of Tokyo Press*, 1979.
- [33] J. R. Hurley, C. A. Tout, and O. R. Pols, “Evolution of binary stars and the effect of tides on binary populations,” *Monthly Notices of the Royal Astronomical Society*, vol. 329, no. 4, pp. 897–928, 2002.
- [34] E. v. d. Heuvel, “Compact stars and the evolution of binary systems,” in *Fluid Flows To Black Holes: A Tribute to S Chandrasekhar on His Birth Centenary*, pp. 55–73, World Scientific, 2011.
- [35] K. Riles, “Recent searches for continuous gravitational waves,” *Modern Physics Letters A*, vol. 32, no. 39, p. 1730035, 2017.
- [36] K. D. Kokkotas and B. G. Schmidt, “Quasi-normal modes of stars and black holes,” *Living Reviews in Relativity*, vol. 2, no. 1, pp. 1–72, 1999.
- [37] P. D. Roy, S. Aneesh, and S. Kar, “Revisiting a family of wormholes: geometry, matter, scalar quasinormal modes and echoes,” *The European Physical Journal C*, vol. 80, no. 9, pp. 1–17, 2020.
- [38] R. Oliveira, D. Dantas, V. Santos, and C. Almeida, “Quasinormal modes of bumblebee wormhole,” *Classical and Quantum Gravity*, vol. 36, no. 10, p. 105013, 2019.
- [39] E. Berti, V. Cardoso, and A. O. Starinets, “Quasinormal modes of black holes and black branes,” *Classical and Quantum Gravity*, vol. 26, no. 16, p. 163001, 2009.
- [40] G. T. Horowitz and V. E. Hubeny, “Quasinormal modes of ads black holes and the approach to thermal equilibrium,” *Physical Review D*, vol. 62, no. 2, p. 024027, 2000.
- [41] N. Heidari, J. Reis, H. Hassanabadi, *et al.*, “The impact of an antisymmetric tensor on charged black holes: evaporation process, geodesics, deflection angle, scattering effects and

- quasinormal modes,” *arXiv preprint arXiv:2404.10721*, 2024.
- [42] B. Hamil and B. C. Lütfüoğlu, “Noncommutative Schwarzschild black hole surrounded by quintessence: Thermodynamics, Shadows and Quasinormal modes,” *Phys. Dark Univ.*, vol. 44, p. 101484, 2024.
- [43] H.-P. Nollert, “Quasinormal modes: the characteristic sound of black holes and neutron stars,” *Classical and Quantum Gravity*, vol. 16, no. 12, p. R159, 1999.
- [44] V. Ferrari and B. Mashhoon, “New approach to the quasinormal modes of a black hole,” *Physical Review D*, vol. 30, no. 2, p. 295, 1984.
- [45] V. Santos, R. V. Maluf, and C. A. S. Almeida, “Quasinormal frequencies of self-dual black holes,” *Physical Review D*, vol. 93, no. 8, p. 084047, 2016.
- [46] A. Övgün, I. Sakalli, and J. Saavedra, “Quasinormal modes of a schwarzschild black hole immersed in an electromagnetic universe,” *Chinese Physics C*, vol. 42, no. 10, p. 105102, 2018.
- [47] K. Jusufi, B. Cuadros-Melgar, G. Leon, A. Jawad, *et al.*, “Charged black holes with yukawa potential,” *arXiv preprint arXiv:2401.15211*, 2024.
- [48] Á. Rincón and V. Santos, “Greybody factor and quasinormal modes of regular black holes,” *The European Physical Journal C*, vol. 80, no. 10, pp. 1–7, 2020.
- [49] A. A. Araújo Filho, K. Jusufi, B. Cuadros-Melgar, and G. Leon, “Dark matter signatures of black holes with yukawa potential,” *Physics of the Dark Universe*, p. 101500, 2024.
- [50] L. London, D. Shoemaker, and J. Healy, “Modeling ringdown: Beyond the fundamental quasinormal modes,” *Physical Review D*, vol. 90, no. 12, p. 124032, 2014.
- [51] M. Maggiore, “Physical interpretation of the spectrum of black hole quasinormal modes,” *Physical Review Letters*, vol. 100, no. 14, p. 141301, 2008.
- [52] A. Flachi and J. P. Lemos, “Quasinormal modes of regular black holes,” *Physical Review D*, vol. 87, no. 2, p. 024034, 2013.
- [53] J. L. Blázquez-Salcedo, X. Y. Chew, and J. Kunz, “Scalar and axial quasinormal modes of massive static phantom wormholes,” *Physical Review D*, vol. 98, no. 4, p. 044035, 2018.
- [54] R. Konoplya and A. Zhidenko, “Quasinormal modes of black holes: From astrophysics to string theory,” *Reviews of Modern Physics*, vol. 83, no. 3, p. 793, 2011.
- [55] A. A. Araújo Filho, J. A. A. S. Reis, and H. Hassanabadi, “Exploring antisymmetric tensor effects on black hole shadows and quasinormal frequencies,” *Journal of Cosmology and*

- Astroparticle Physics*, vol. 2024, no. 05, p. 029, 2024.
- [56] C. O. Lee, J. Y. Kim, and M.-I. Park, “Quasi-normal modes and stability of einstein–born–infeld black holes in de sitter space,” *The European Physical Journal C*, vol. 80, no. 8, pp. 1–21, 2020.
- [57] A. Jawad, S. Chaudhary, M. Yasir, A. Övgün, and İ. Sakallı, “Quasinormal modes of extended gravity black holes through higher order wkb method,” *International Journal of Geometric Methods in Modern Physics*, p. 2350129, 2023.
- [58] S. Fernando and J. Correa, “Quasinormal Modes of Bardeen Black Hole: Scalar Perturbations,” *Phys. Rev. D*, vol. 86, p. 064039, 2012.
- [59] L. Hui, D. Kabat, and S. S. Wong, “Quasinormal modes, echoes and the causal structure of the green’s function,” *Journal of Cosmology and Astroparticle Physics*, vol. 2019, no. 12, p. 020, 2019.
- [60] R. Maluf, C. Almeida, R. Casana, and M. Ferreira Jr, “Einstein-hilbert graviton modes modified by the lorentz-violating bumblebee field,” *Physical Review D*, vol. 90, no. 2, p. 025007, 2014.
- [61] M. Cadoni, M. Oi, and A. P. Sanna, “Quasi-normal modes and microscopic description of 2d black holes,” *Journal of High Energy Physics*, vol. 2022, no. 1, pp. 1–23, 2022.
- [62] M. Okyay and A. Övgün, “Nonlinear electrodynamics effects on the black hole shadow, deflection angle, quasinormal modes and greybody factors,” *Journal of Cosmology and Astroparticle Physics*, vol. 2022, no. 01, p. 009, 2022.
- [63] R. G. Daghigh and M. D. Green, “Highly Real, Highly Damped, and Other Asymptotic Quasinormal Modes of Schwarzschild-Anti De Sitter Black Holes,” *Class. Quant. Grav.*, vol. 26, p. 125017, 2009.
- [64] Y. Zhao, X. Ren, A. Ilyas, E. N. Saridakis, and Y.-F. Cai, “Quasinormal modes of black holes in  $f(t)$  gravity,” *Journal of Cosmology and Astroparticle Physics*, vol. 2022, no. 10, p. 087, 2022.
- [65] D. J. Gogoi, A. Övgün, and M. Koussour, “Quasinormal modes of black holes in  $f(Q)$  gravity,” *Eur. Phys. J. C*, vol. 83, no. 8, p. 700, 2023.
- [66] S. Boudet, F. Bombacigno, G. J. Olmo, and P. J. Porfirio, “Quasinormal modes of schwarzschild black holes in projective invariant chern-simons modified gravity,” *Journal of Cosmology and Astroparticle Physics*, vol. 2022, no. 05, p. 032, 2022.



- [67] R. G. Daghigh, M. D. Green, and G. Kunstatter, “Scalar Perturbations and Stability of a Loop Quantum Corrected Kruskal Black Hole,” *Phys. Rev. D*, vol. 103, no. 8, p. 084031, 2021.
- [68] A. A. Araújo Filho, “Implications of a simpson–visser solution in verlinde’s framework,” *The European Physical Journal C*, vol. 84, no. 1, pp. 1–22, 2024.
- [69] R. G. Daghigh, M. D. Green, and J. C. Morey, “Calculating quasinormal modes of Schwarzschild anti–de Sitter black holes using the continued fraction method,” *Phys. Rev. D*, vol. 107, no. 2, p. 024023, 2023.
- [70] R. G. Daghigh, M. D. Green, and J. C. Morey, “Significance of Black Hole Quasinormal Modes: A Closer Look,” *Phys. Rev. D*, vol. 101, no. 10, p. 104009, 2020.
- [71] A. A. Araújo Filho, “Analysis of a regular black hole in verlinde’s gravity,” *Classical and Quantum Gravity*, vol. 41, no. 1, p. 015003, 2023.
- [72] S. Fernando, “Quasinormal modes of dilaton-de Sitter black holes: scalar perturbations,” *Gen. Rel. Grav.*, vol. 48, no. 3, p. 24, 2016.
- [73] N. Heidari, H. Hassanabadi, A. A. Araújo Filho, J. Kříž, S. Zare, and P. J. Porfírio, “Gravitational signatures of a non–commutative stable black hole,” *Physics of the Dark Universe*, vol. 43, p. 101382, 2023.
- [74] R. G. Daghigh, M. D. Green, J. C. Morey, and G. Kunstatter, “Scalar Perturbations of a Single-Horizon Regular Black Hole,” *Phys. Rev. D*, vol. 102, no. 10, p. 104040, 2020.
- [75] D. Liu, Y. Yang, A. Övgün, Z.-W. Long, and Z. Xu, “The quasinormal modes and greybody bounds of rotating black holes in a dark matter halo,” *arXiv preprint arXiv:2204.11563*, 2022.
- [76] Y. Yang, D. Liu, A. Övgün, Z.-W. Long, and Z. Xu, “Probing hairy black holes caused by gravitational decoupling using quasinormal modes and greybody bounds,” *Physical Review D*, vol. 107, no. 6, p. 064042, 2023.
- [77] D. J. Gogoi, A. Övgün, and D. Demir, “Quasinormal modes and greybody factors of symmergent black hole,” *Phys. Dark Univ.*, vol. 42, p. 101314, 2023.
- [78] R. Maluf, V. Santos, W. Cruz, and C. Almeida, “Matter-gravity scattering in the presence of spontaneous lorentz violation,” *Physical Review D*, vol. 88, no. 2, p. 025005, 2013.
- [79] J. Y. Kim, C. O. Lee, and M.-I. Park, “Quasi-normal modes of a natural ads wormhole in einstein–born–infeld gravity,” *The European Physical Journal C*, vol. 78, no. 12, pp. 1–15,

- 2018.
- [80] R. G. Daghigh and G. Kunstatter, “Highly damped quasinormal modes of generic single horizon black holes,” *Class. Quant. Grav.*, vol. 22, pp. 4113–4128, 2005.
  - [81] G. Lambiase, R. C. Pantig, D. J. Gogoi, and A. Övgün, “Investigating the connection between generalized uncertainty principle and asymptotically safe gravity in black hole signatures through shadow and quasinormal modes,” *arXiv preprint arXiv:2304.00183*, 2023.
  - [82] A. A. Araújo Filho, H. Hassanabadi, N. Heidari, J. Kríz, and S. Zare, “Gravitational traces of bumblebee gravity in metric-affine formalism,” *Class. Quant. Grav.*, vol. 41, p. 055003, 2024.
  - [83] Y. Yang, D. Liu, A. Övgün, Z.-W. Long, and Z. Xu, “Probing hairy black holes caused by gravitational decoupling using quasinormal modes and greybody bounds,” *Phys. Rev. D*, vol. 107, no. 6, p. 064042, 2023.
  - [84] D. J. Gogoi, A. Övgün, and M. Koussour, “Quasinormal modes of black holes in  $f(q)$  gravity,” *arXiv preprint arXiv:2303.07424*, 2023.
  - [85] F. Eisenhauer, R. Genzel, T. Alexander, R. Abuter, T. Paumard, T. Ott, A. Gilbert, S. Gillessen, M. Horrobin, S. Trippe, *et al.*, “Sinfoni in the galactic center: young stars and infrared flares in the central light-month,” *The Astrophysical Journal*, vol. 628, no. 1, p. 246, 2005.
  - [86] E. H. T. Collaboration *et al.*, “First m87 event horizon telescope results. iv. imaging the central supermassive black hole,” *arXiv preprint arXiv:1906.11241*, 2019.
  - [87] K. Akiyama, A. Alberdi, W. Alef, K. Asada, R. Azulay, A.-K. Baczkó, D. Ball, M. Baloković, J. Barrett, D. Bintley, *et al.*, “First m87 event horizon telescope results. ii. array and instrumentation,” *The Astrophysical Journal Letters*, vol. 875, no. 1, p. L2, 2019.
  - [88] K. Akiyama, A. Alberdi, W. Alef, K. Asada, R. Azulay, A.-K. Baczkó, D. Ball, M. Baloković, J. Barrett, D. Bintley, *et al.*, “First m87 event horizon telescope results. v. physical origin of the asymmetric ring,” *The Astrophysical Journal Letters*, vol. 875, no. 1, p. L5, 2019.
  - [89] E. H. T. Collaboration *et al.*, “First m87 event horizon telescope results. iv. imaging the central supermassive black hole,” *arXiv preprint arXiv:1906.11241*, 2019.
  - [90] K. Akiyama, A. Alberdi, W. Alef, K. Asada, R. Azulay, A.-K. Baczkó, D. Ball, M. Baloković, J. Barrett, D. Bintley, *et al.*, “First m87 event horizon telescope results. v. physical origin of the asymmetric ring,” *The Astrophysical Journal Letters*, vol. 875, no. 1, p. L5, 2019.

- [91] D. Ball, C.-K. Chan, P. Christian, B. T. Jannuzi, J. Kim, D. P. Marrone, L. Medeiros, F. Ozel, D. Psaltis, M. Rose, *et al.*, “First m87 event horizon telescope results. vi. the shadow and mass of the central black hole,” 2019.
- [92] R. C. Pantig, A. Övgün, and D. Demir, “Testing symmergent gravity through the shadow image and weak field photon deflection by a rotating black hole using the m87 and sgr. a results,” *The European Physical Journal C*, vol. 83, no. 3, p. 250, 2023.
- [93] İ. Çimdiker, D. Demir, and A. Övgün, “Black hole shadow in symmergent gravity,” *Physics of the Dark Universe*, vol. 34, p. 100900, 2021.
- [94] R. C. Pantig, L. Mastrototaro, G. Lambiase, and A. Övgün, “Shadow, lensing and neutrino propagation by dyonic modmax black holes,” *arXiv preprint arXiv:2208.06664*, 2022.
- [95] K. S. Virbhadra and G. F. Ellis, “Schwarzschild black hole lensing,” *Phys. Rev. D*, vol. 62, no. 8, p. 084003, 2000.
- [96] V. Perlick, “Theoretical gravitational lensing—beyond the weak-field small-angle approximation,” in *The Eleventh Marcel Grossmann Meeting: On Recent Developments in Theoretical and Experimental General Relativity, Gravitation and Relativistic Field Theories (In 3 Volumes)*, pp. 680–699, World Scientific, 2008.
- [97] S. Frittelli, T. P. Kling, and E. T. Newman, “Spacetime perspective of schwarzschild lensing,” *Phys. Rev. D*, vol. 61, no. 6, p. 064021, 2000.
- [98] V. Bozza, S. Capozziello, G. Iovane, and G. Scarpetta, “Strong field limit of black hole gravitational lensing,” *General Relativity and Gravitation*, vol. 33, pp. 1535–1548, 2001.
- [99] N. Tsukamoto, “Deflection angle in the strong deflection limit in a general asymptotically flat, static, spherically symmetric spacetime,” *Phys. Rev. D*, vol. 95, no. 6, p. 064035, 2017.
- [100] N. Tsukamoto, Y. Gong, *et al.*, “Retrolensing by a charged black hole,” *Phys. Rev. D*, vol. 95, no. 6, p. 064034, 2017.
- [101] A. A. Araújo Filho, “Remarks on a nonlinear electromagnetic extension in ads reissner-nordström spacetime,” *arXiv preprint arXiv:2410.23165*, 2024.
- [102] E. F. Eiroa, G. E. Romero, and D. F. Torres, “Reissner-nordström black hole lensing,” *Physical Review D*, vol. 66, no. 2, p. 024010, 2002.
- [103] A. A. Araújo Filho, “Static limit analysis of a nonlinear electromagnetic generalization of the kerr-newman black hole,” *arXiv preprint arXiv:2410.12060*, 2024.

- [104] E. F. Eiroa and D. F. Torres, “Strong field limit analysis of gravitational retrolensing,” *Phys. Rev. D*, vol. 69, no. 6, p. 063004, 2004.
- [105] V. Bozza, F. De Luca, and G. Scarpetta, “Kerr black hole lensing for generic observers in the strong deflection limit,” *Phys. Rev. D*, vol. 74, no. 6, p. 063001, 2006.
- [106] S. E. Vazquez and E. P. Esteban, “Strong field gravitational lensing by a kerr black hole,” *arXiv preprint gr-qc/0308023*, 2003.
- [107] A. B. Aazami, C. R. Keeton, and A. Petters, “Lensing by kerr black holes. ii: Analytical study of quasi-equatorial lensing observables,” *J. Math. Phys.*, vol. 52, no. 10, 2011.
- [108] V. Bozza, “Quasiequatorial gravitational lensing by spinning black holes in the strong field limit,” *Physical Review D*, vol. 67, no. 10, p. 103006, 2003.
- [109] V. Bozza and G. Scarpetta, “Strong deflection limit of black hole gravitational lensing with arbitrary source distances,” *Phys. Rev. D*, vol. 76, no. 8, p. 083008, 2007.
- [110] V. Bozza, F. De Luca, G. Scarpetta, and M. Sereno, “Analytic kerr black hole lensing for equatorial observers in the strong deflection limit,” *Phys. Rev. D*, vol. 72, no. 8, p. 083003, 2005.
- [111] N. Tsukamoto, “Retrolensing by a wormhole at deflection angles  $\pi$  and  $3\pi$ ,” *Phys. Rev. D*, vol. 95, no. 8, p. 084021, 2017.
- [112] R. Shaikh, P. Banerjee, S. Paul, and T. Sarkar, “Strong gravitational lensing by wormholes,” *JCAP*, vol. 2019, no. 07, p. 028, 2019.
- [113] N. Tsukamoto, “Strong deflection limit analysis and gravitational lensing of an ellis wormhole,” *Phys. Rev. D*, vol. 94, no. 12, p. 124001, 2016.
- [114] G. W. Gibbons and M. Vyska, “The application of weierstrass elliptic functions to schwarzschild null geodesics,” *Class. Quant. Grav.*, vol. 29, no. 6, p. 065016, 2012.
- [115] N. Tsukamoto, T. Harada, and K. Yajima, “Can we distinguish between black holes and wormholes by their einstein-ring systems?,” *Phys. Rev. D*, vol. 86, no. 10, p. 104062, 2012.
- [116] R. Shaikh and S. Kar, “Gravitational lensing by scalar-tensor wormholes and the energy conditions,” *Phys. Rev. D*, vol. 96, no. 4, p. 044037, 2017.
- [117] O. Donmez, “Bondi-Hoyle-Lyttleton accretion around the rotating hairy Horndeski black hole,” *JCAP*, vol. 09, p. 006, 2024.
- [118] F. Koyuncu and O. Dönmez, “Numerical simulation of the disk dynamics around the black hole: Bondi Hoyle accretion,” *Mod. Phys. Lett. A*, vol. 29, p. 1450115, 2014.

- [119] O. Donmez, “Perturbing the Stable Accretion Disk in Kerr and 4D Einstein–Gauss–Bonnet Gravities: Comprehensive Analysis of Instabilities and Dynamics,” *Res. Astron. Astrophys.*, vol. 24, no. 8, p. 085001, 2024.
- [120] S. W. Hawking, “Black hole explosions?,” *Nature*, vol. 248, no. 5443, pp. 30–31, 1974.
- [121] S. W. Hawking, “Particle creation by black holes,” *Communications in mathematical physics*, vol. 43, no. 3, pp. 199–220, 1975.
- [122] S. W. Hawking, “Black holes and thermodynamics,” *Physical Review D*, vol. 13, no. 2, p. 191, 1976.
- [123] A. Övgün and I. Sakalli, “Hawking Radiation via Gauss-Bonnet Theorem,” *Annals Phys.*, vol. 413, p. 168071, 2020.
- [124] G. W. Gibbons and S. W. Hawking, “Cosmological event horizons, thermodynamics, and particle creation,” *Physical Review D*, vol. 15, no. 10, p. 2738, 1977.
- [125] X.-M. Kuang, B. Liu, and A. Övgün, “Nonlinear electrodynamics AdS black hole and related phenomena in the extended thermodynamics,” *Eur. Phys. J. C*, vol. 78, no. 10, p. 840, 2018.
- [126] X.-M. Kuang, J. Saavedra, and A. Övgün, “The Effect of the Gauss-Bonnet term to Hawking Radiation from arbitrary dimensional Black Brane,” *Eur. Phys. J. C*, vol. 77, no. 9, p. 613, 2017.
- [127] A. Övgün and K. Jusufi, “Massive vector particles tunneling from noncommutative charged black holes and their GUP-corrected thermodynamics,” *Eur. Phys. J. Plus*, vol. 131, no. 5, p. 177, 2016.
- [128] A. Övgün, I. Sakalli, J. Saavedra, and C. Leiva, “Shadow cast of noncommutative black holes in Rastall gravity,” *Mod. Phys. Lett. A*, vol. 35, no. 20, p. 2050163, 2020.
- [129] P. Sedaghatnia, H. Hassanabadi, J. Porfírio, W. Chung, *et al.*, “Thermodynamical properties of a deformed schwarzschild black hole via dunkl generalization,” *arXiv preprint arXiv:2302.11460*, 2023.
- [130] B. Harms and Y. Leblanc, “Statistical mechanics of black holes,” *Physical Review D*, vol. 46, no. 6, p. 2334, 1992.
- [131] A. Jawad and A. Khawer, “Thermodynamic consequences of well-known regular black holes under modified first law,” *The European Physical Journal C*, vol. 78, pp. 1–10, 2018.
- [132] D. Hansen, D. Kubizňák, and R. B. Mann, “Criticality and surface tension in rotating horizon thermodynamics,” *Classical and Quantum Gravity*, vol. 33, no. 16, p. 165005, 2016.

- [133] A. A. Araújo Filho, “Analysis of a regular black hole in verlinde’s gravity,” *Classical and Quantum Gravity*, vol. 41, no. 1, p. 015003, 2023.
- [134] D. Hansen, D. Kubizňák, and R. B. Mann, “Universality of p- v criticality in horizon thermodynamics,” *Journal of High Energy Physics*, vol. 2017, no. 1, pp. 1–24, 2017.
- [135] A. A. Araújo Filho, “Implications of a simpson–visser solution in verlinde’s framework,” *The European Physical Journal C*, vol. 84, no. 1, pp. 1–22, 2024.
- [136] C. Vaz, “Canonical quantization and the statistical entropy of the schwarzschild black hole,” *Physical Review D*, vol. 61, no. 6, p. 064017, 2000.
- [137] D. Chen, J. Tao, *et al.*, “The modified first laws of thermodynamics of anti-de sitter and de sitter space–times,” *Nuclear Physics B*, vol. 918, pp. 115–128, 2017.
- [138] P. Kraus and F. Wilczek, “Self-interaction correction to black hole radiance,” *Nuclear Physics B*, vol. 433, no. 2, pp. 403–420, 1995.
- [139] K. Jusufi, İ. Sakallı, and A. Övgün, “Effect of lorentz symmetry breaking on the deflection of light in a cosmic string spacetime,” *Phys. Rev. D*, vol. 96, no. 2, p. 024040, 2017.
- [140] M. Parikh, “A secret tunnel through the horizon,” *International Journal of Modern Physics D*, vol. 13, no. 10, pp. 2351–2354, 2004.
- [141] M. Anacleto, F. Brito, and E. Passos, “Quantum-corrected self-dual black hole entropy in tunneling formalism with gup,” *Physics Letters B*, vol. 749, pp. 181–186, 2015.
- [142] A. Medved, “Radiation via tunneling from a de sitter cosmological horizon,” *Physical Review D*, vol. 66, no. 12, p. 124009, 2002.
- [143] F. Mirekhtiary, A. Abbasi, K. Hosseini, and F. Tulucu, “Tunneling of rotational black string with nonlinear electromagnetic fields,” *Physica Scripta*, vol. 99, no. 3, p. 035005, 2024.
- [144] C. Silva and F. Brito, “Quantum tunneling radiation from self-dual black holes,” *Physics Letters B*, vol. 725, no. 4-5, pp. 456–462, 2013.
- [145] F. Del Porro, S. Liberati, and M. Schneider, “Tunneling method for hawking quanta in analogue gravity,” *arXiv preprint arXiv:2406.14603*, 2024.
- [146] X. Calmet, S. D. Hsu, and M. Sebastianutti, “Quantum gravitational corrections to particle creation by black holes,” *Physics Letters B*, vol. 841, p. 137820, 2023.
- [147] G. Johnson and J. March-Russell, “Hawking radiation of extended objects,” *Journal of High Energy Physics*, vol. 2020, no. 4, pp. 1–16, 2020.

- [148] L. Vanzo, G. Acquaviva, and R. Di Criscienzo, “Tunnelling methods and hawking’s radiation: achievements and prospects,” *Classical and Quantum Gravity*, vol. 28, no. 18, p. 183001, 2011.
- [149] P. Mitra, “Hawking temperature from tunnelling formalism,” *Physics Letters B*, vol. 648, no. 2-3, pp. 240–242, 2007.
- [150] J. Zhang and Z. Zhao, “New coordinates for kerr–newman black hole radiation,” *Physics Letters B*, vol. 618, no. 1-4, pp. 14–22, 2005.
- [151] A. Touati and Z. Slimane, “Quantum tunneling from schwarzschild black hole in non-commutative gauge theory of gravity,” *Physics Letters B*, vol. 848, p. 138335, 2024.
- [152] D. Senjaya, “The bocharova–bronnikov–melnikov–bekenstein black hole’s exact quasibound states and hawking radiation,” *The European Physical Journal C*, vol. 84, no. 6, p. 607, 2024.
- [153] A. I. Janis and E. T. Newman, “Structure of gravitational sources,” *Journal of Mathematical Physics*, vol. 6, no. 6, pp. 902–914, 1965.
- [154] E. T. Newman and A. Janis, “Note on the kerr spinning-particle metric,” *Journal of Mathematical Physics*, vol. 6, no. 6, pp. 915–917, 1965.
- [155] M. Afrin, S. G. Ghosh, and A. Wang, “Testing egb gravity coupled to bumblebee field and black hole parameter estimation with eht observations,” *Physics of the Dark Universe*, vol. 46, p. 101642, 2024.
- [156] M. Azreg-Aïnou, “Generating rotating regular black hole solutions without complexification,” *Physical Review D*, vol. 90, no. 6, p. 064041, 2014.
- [157] M. Azreg-Aïnou, “From static to rotating to conformal static solutions: rotating imperfect fluid wormholes with (out) electric or magnetic field,” *The European Physical Journal C*, vol. 74, pp. 1–11, 2014.
- [158] S. G. Ghosh and S. D. Maharaj, “Radiating kerr-like regular black hole,” *The European Physical Journal C*, vol. 75, pp. 1–9, 2015.
- [159] C. Bambi and L. Modesto, “Rotating regular black holes,” *Physics Letters B*, vol. 721, no. 4-5, pp. 329–334, 2013.
- [160] T. Johannsen and D. Psaltis, “Metric for rapidly spinning black holes suitable for strong-field tests of the no-hair theorem,” *Physical Review D—Particles, Fields, Gravitation, and Cosmology*, vol. 83, no. 12, p. 124015, 2011.
- [161] S. G. Ghosh, “Rotating black hole and quintessence,” *The European Physical Journal C*, vol. 76, no. 4, p. 222, 2016.

- [162] S. G. Ghosh, “A nonsingular rotating black hole,” *The European Physical Journal C*, vol. 75, no. 11, p. 532, 2015.
- [163] K. Jusufi, M. Jamil, H. Chakrabarty, Q. Wu, C. Bambi, and A. Wang, “Rotating regular black holes in conformal massive gravity,” *Physical Review D*, vol. 101, no. 4, p. 044035, 2020.
- [164] M. Chaichian, A. Tureanu, and G. Zet, “Corrections to schwarzschild solution in noncommutative gauge theory of gravity,” *Physics Letters B*, vol. 660, no. 5, pp. 573–578, 2008.
- [165] G. Zet, V. Manta, and S. Babeti, “Desitter gauge theory of gravitation,” *International Journal of Modern Physics C*, vol. 14, no. 01, pp. 41–48, 2003.
- [166] O. Bertolami and J. Paramos, “Vacuum solutions of a gravity model with vector-induced spontaneous lorentz symmetry breaking,” *Phys. Rev. D*, vol. 72, no. 4, p. 044001, 2005.
- [167] A. H. Chamseddine, “Deforming einstein’s gravity,” *Physics Letters B*, vol. 504, no. 1-2, pp. 33–37, 2001.
- [168] B. Jurco, S. Schraml, P. Schupp, and J. Wess, “Enveloping algebra-valued gauge transformations for non-abelian gauge groups on non-commutative spaces,” *The European Physical Journal C-Particles and Fields*, vol. 17, no. 3, pp. 521–526, 2000.
- [169] N. Heidari, H. Hassanabadi, A. A. Araújo Filho, J. Kriz, S. Zare, and P. J. Porfírio, “Gravitational signatures of a non-commutative stable black hole,” *Physics of the Dark Universe*, p. 101382, 2023.
- [170] N. Heidari, A. Övgün, *et al.*, “Quantum gravity effects on particle creation and evaporation in a non-commutative black hole via mass deformation,” *arXiv preprint arXiv:2409.03566*, 2024.
- [171] M. Azreg-Aïnou, “Generating rotating regular black hole solutions without complexification,” *Physical Review D*, vol. 90, no. 6, p. 064041, 2014.
- [172] R. Kumar and S. G. Ghosh, “Rotating black holes in 4d einstein-gauss-bonnet gravity and its shadow,” *Journal of Cosmology and Astroparticle Physics*, vol. 2020, no. 07, p. 053, 2020.
- [173] S. Brahma, C.-Y. Chen, and D.-h. Yeom, “Testing loop quantum gravity from observational consequences of nonsingular rotating black holes,” *Physical Review Letters*, vol. 126, no. 18, p. 181301, 2021.
- [174] S. U. Islam, J. Kumar, R. K. Walia, and S. G. Ghosh, “Investigating loop quantum gravity with event horizon telescope observations of the effects of rotating black holes,” *The*



- Astrophysical Journal*, vol. 943, no. 1, p. 22, 2023.
- [175] M. Afrin and S. G. Ghosh, “Testing horndeski gravity from eht observational results for rotating black holes,” *The Astrophysical Journal*, vol. 932, no. 1, p. 51, 2022.
- [176] M. Visser, “The kerr spacetime: A brief introduction,” *arXiv preprint arXiv:0706.0622*, 2007.
- [177] D. Grumiller and M. M. Sheikh-Jabbari, *Black hole physics*. Springer, 2022.
- [178] D. Christodoulou and R. Ruffini, “Reversible transformations of a charged black hole,” *Physical Review D*, vol. 4, no. 12, p. 3552, 1971.
- [179] O. Ruiz, U. Molina, and P. Vitoria, “Thermodynamic analysis of kerr-newman black holes,” in *Journal of Physics: Conference Series*, vol. 1219, p. 012016, IOP Publishing, 2019.
- [180] R. M. Wald, *General relativity*. University of Chicago press, 2010.
- [181] J. M. Bardeen, B. Carter, and S. W. Hawking, “The four laws of black hole mechanics,” *Communications in mathematical physics*, vol. 31, pp. 161–170, 1973.
- [182] D. N. Page, “Hawking radiation and black hole thermodynamics,” *New Journal of Physics*, vol. 7, no. 1, p. 203, 2005.
- [183] S. Carlip, “Black hole thermodynamics,” *International Journal of Modern Physics D*, vol. 23, no. 11, p. 1430023, 2014.
- [184] P. C. Davies, “Thermodynamics of black holes,” *Reports on Progress in Physics*, vol. 41, no. 8, p. 1313, 1978.
- [185] S. W. Hawking, “Black holes and thermodynamics,” *Physical Review D*, vol. 13, no. 2, p. 191, 1976.
- [186] D. Christodoulou, “Reversible and irreversible transformations in black-hole physics,” *Physical Review Letters*, vol. 25, no. 22, p. 1596, 1970.
- [187] J. D. Bekenstein, “Black holes and the second law,” in *JACOB BEKENSTEIN: The Conservative Revolutionary*, pp. 303–306, World Scientific, 2020.
- [188] J. D. Bekenstein, “Generalized second law of thermodynamics in black-hole physics,” *Physical Review D*, vol. 9, no. 12, p. 3292, 1974.
- [189] A. Hrelja, T. Jurić, and F. Požar, “Entropy of black holes, charged probes and noncommutative generalization,” *arXiv preprint arXiv:2407.13233*, 2024.
- [190] M. D. Ćirić, N. Konjik, and A. Samsarov, “Noncommutative scalar quasinormal modes of the reissner–nordström black hole,” *Classical and quantum gravity*, vol. 35, no. 17, p. 175005, 2018.

- [191] M. D. Ćirić, T. Jurić, N. Konjik, A. Samsarov, and I. Smolić, “Noncommutative reissner-nordström black hole from noncommutative charged scalar field,” *arXiv preprint arXiv:2404.03755*, 2024.
- [192] M. Dimitrijević Ćirić, N. Konjik, and A. Samsarov, “Noncommutative scalar field in the nonextremal reissner-nordström background: Quasinormal mode spectrum,” *Physical Review D*, vol. 101, no. 11, p. 116009, 2020.
- [193] T. Jurić and F. Požar, “Noncommutative correction to the entropy of charged btz black hole,” *Symmetry*, vol. 15, no. 2, p. 417, 2023.
- [194] R. P. Kerr, “Gravitational field of a spinning mass as an example of algebraically special metrics,” *Physical review letters*, vol. 11, no. 5, p. 237, 1963.
- [195] Q.-Q. Jiang, S.-Q. Wu, and X. Cai, “Hawking radiation as tunneling from the kerr and kerr-newman black holes,” *Physical Review D—Particles, Fields, Gravitation, and Cosmology*, vol. 73, no. 6, p. 064003, 2006.
- [196] J. Zhang and Z. Zhao, “Hawking radiation via tunneling from kerr black holes,” *Modern Physics Letters A*, vol. 20, no. 22, pp. 1673–1681, 2005.
- [197] R. Li, J.-R. Ren, and S.-W. Wei, “Hawking radiation of dirac particles via tunneling from the kerr black hole,” *Classical and Quantum Gravity*, vol. 25, no. 12, p. 125016, 2008.
- [198] I. Agullo, J. Navarro-Salas, G. J. Olmo, and L. Parker, “Hawking radiation by kerr black holes and conformal symmetry,” *Physical review letters*, vol. 105, no. 21, p. 211305, 2010.
- [199] K. Murata and J. Soda, “Hawking radiation from rotating black holes and gravitational anomalies,” *Physical Review D—Particles, Fields, Gravitation, and Cosmology*, vol. 74, no. 4, p. 044018, 2006.
- [200] C. Corda, S. Hendi, R. Katebi, and N. Schmidt, “Effective state, hawking radiation and quasi-normal modes for kerr black holes,” *Journal of High Energy Physics*, vol. 2013, no. 6, pp. 1–12, 2013.
- [201] Z. Xu and B. Chen, “Hawking radiation from general kerr-(anti) de sitter black holes,” *Physical Review D—Particles, Fields, Gravitation, and Cosmology*, vol. 75, no. 2, p. 024041, 2007.
- [202] K. Umetsu, “Hawking radiation from kerr–newman black hole and tunneling mechanism,” *International journal of modern physics A*, vol. 25, no. 21, pp. 4123–4140, 2010.

- [203] A. Arbey, J. Auffinger, and J. Silk, “Evolution of primordial black hole spin due to hawking radiation,” *Monthly Notices of the Royal Astronomical Society*, vol. 494, no. 1, pp. 1257–1262, 2020.
- [204] L. Wang and R. Li, “Entanglement islands and the page curve of hawking radiation for rotating kerr black holes,” *Physical Review D*, vol. 110, no. 6, p. 066012, 2024.
- [205] T. McMaken and A. J. Hamilton, “Hawking radiation inside a rotating black hole,” *Physical Review D*, vol. 109, no. 6, p. 065023, 2024.
- [206] D. Senjaya, “The kerr–bumblebee exact massive and massless scalar quasibound states and hawking radiation,” *The European Physical Journal C*, vol. 84, no. 4, p. 424, 2024.
- [207] M. Angheben, M. Nadalini, L. Vanzo, and S. Zerbini, “Hawking radiation as tunneling for extremal and rotating black holes,” *Journal of High Energy Physics*, vol. 2005, no. 05, p. 014, 2005.
- [208] R. Kerner and R. B. Mann, “Tunnelling, temperature, and taub-nut black holes,” *Physical Review D—Particles, Fields, Gravitation, and Cosmology*, vol. 73, no. 10, p. 104010, 2006.
- [209] R. Kerner and R. B. Mann, “Fermions tunnelling from black holes,” *Classical and Quantum Gravity*, vol. 25, no. 9, p. 095014, 2008.
- [210] R. Di Criscienzo and L. Vanzo, “Fermion tunneling from dynamical horizons,” *Europhysics Letters*, vol. 82, no. 6, p. 60001, 2008.
- [211] P. Mitra, “Hawking temperature from tunnelling formalism,” *Physics Letters B*, vol. 648, no. 2-3, pp. 240–242, 2007.
- [212] E. T. Akhmedov, V. Akhmedova, and D. Singleton, “Hawking temperature in the tunneling picture,” *Physics Letters B*, vol. 642, no. 1-2, pp. 124–128, 2006.
- [213] T. Damour and R. Ruffini, “Black-hole evaporation in the klein-sauter-heisenberg-euler formalism,” *Physical Review D*, vol. 14, no. 2, p. 332, 1976.
- [214] S. Sannan, “Heuristic derivation of the probability distributions of particles emitted by a black hole,” *General Relativity and Gravitation*, vol. 20, pp. 239–246, 1988.
- [215] R. M. Wald, *General Relativity*. Chicago, USA: Chicago Univ. Pr., 1984.
- [216] A. Anjum, M. Afrin, and S. G. Ghosh, “Investigating effects of dark matter on photon orbits and black hole shadows,” *Physics of the Dark Universe*, vol. 40, p. 101195, 2023.
- [217] E. Teo, “Spherical orbits around a kerr black hole,” *General Relativity and Gravitation*, vol. 53, no. 1, p. 10, 2021.

- [218] T. Hsieh, D.-S. Lee, and C.-Y. Lin, “Strong gravitational lensing by kerr and kerr-newman black holes,” *Physical Review D*, vol. 103, no. 10, p. 104063, 2021.
- [219] Y.-W. Hsiao, D.-S. Lee, and C.-Y. Lin, “Equatorial light bending around kerr-newman black holes,” *Physical Review D*, vol. 101, no. 6, p. 064070, 2020.
- [220] S. V. Iyer and E. C. Hansen, “Light’s bending angle in the equatorial plane of a kerr black hole,” *Physical Review D—Particles, Fields, Gravitation, and Cosmology*, vol. 80, no. 12, p. 124023, 2009.
- [221] N. Tsukamoto, “Deflection angle in the strong deflection limit in a general asymptotically flat, static, spherically symmetric spacetime,” *Phys. Rev. D*, vol. 95, no. 6, p. 064035, 2017.
- [222] V. Bozza, “Gravitational lensing in the strong field limit,” *Phys. Rev. D*, vol. 66, no. 10, p. 103001, 2002.
- [223] A. A. Araújo Filho, “How does non-metricity affect particle creation and evaporation in bumblebee gravity?,” *arXiv preprint arXiv:2501.00927*, 2025.
- [224] A. A. Araújo Filho, “Particle creation and evaporation in kalb-ramond gravity,” *arXiv preprint arXiv:2411.06841*, 2024.